Sources and Sinks of Isoprene in the Global Open Ocean: Simulated Patterns and Emissions to the Atmosphere

Ludivine Conte, Sophie Laval-Szopa, Olivier Aumont, Valérie Gros, Laurent Bopp

JGR Oceans

RESEARCH ARTICLE
10.1029/2019JC015946

Sources and Sinks of Isoprene in the Global Open Ocean: Simulated Patterns and Emissions to the Atmosphere

Ludivine Conte[1], Sophie Szopa[1], Olivier Aumont[2], Valérie Gros[1], and Laurent Bopp[3]

[1]Laboratoire des Sciences du Climat et de l'Environnement, IPSL, CEA/CNRS/UVSQ, Gif sur Yvette, France, [2]Laboratoire d'Océanographie et de Climatologie: Expérimentation et Approches Numériques, IPSL, Paris, France, [3]Laboratoire de Météorologie Dynamique, IPSL, Ecole Normale Supérieure/PSL Research University/CNRS/Ecole Polytechnique/Sorbonne Université, Paris, France

Key Points:
- We developed a mechanistic representation of the marine isoprene cycle in a 3D ocean biogeochemical model
- The effect of temperature on biological production and the inclusion of a variable bacterial consumption rate are key to reproduce observed isoprene concentrations
- The marine isoprene source to the atmosphere is estimated at 0.66 (0.43–0.82) Tg C yr^{-1}, with a significant contribution from isoprene production below the mixed layer

Supporting Information:
- Supporting Information S1

Correspondence to:
L. Conte,
ludivine.conte@lsce.ipsl.fr

Citation:
Conte, L., Szopa, S., Aumont, O., Gros, V., & Bopp, L. (2020). Sources and sinks of isoprene in the global open ocean: Simulated patterns and emissions to the atmosphere. *Journal of Geophysical Research: Oceans*, *125*, e2019JC015946. https://doi.org/10.1029/2019JC015946

Received 5 DEC 2019
Accepted 15 MAY 2020
Accepted article online 22 MAY 2020

Abstract The ocean is a source of isoprene to the atmosphere. Although their global estimates are relatively low compared with the terrestrial source, these emissions have an influence on atmospheric chemistry. The lack of knowledge about the sources and sinks of isoprene in the ocean has hitherto precluded a precise assessment of when and where these emissions might be significant. Here we use the general circulation and biogeochemistry model *Nucleus for European Modelling of the Ocean, Pelagic Interaction Scheme for Carbon and Ecosystem Studies* (NEMO-PISCES) to explore different parameterizations of the 3D oceanic sources and sinks of isoprene. In addition, we investigate a representation of the isoprene emission due to photoproduction in the sea surface microlayer. Our model estimates are complemented by a new data compilation of laboratory isoprene production rates and in situ isoprene concentrations. This study constitutes the first attempt to simulate isoprene in a global 3D ocean biogeochemical model. We find that sea surface temperature is an important driver modulating phytoplankton isoprene production and that light levels only play a secondary role at the scale of the global ocean. Furthermore, the use of a variable biochemical consumption rate improves the model-data comparison. We show the importance of isoprene production below the mixed layer and, as a consequence, demonstrate that models based on 2D surface satellite chlorophyll-a could miss up to 18.5% of oceanic isoprene emissions. The oceanic isoprene emissions to the atmosphere are estimated to 0.66 (0.43–0.82) Tg C yr^{-1} in the low range of previous estimates.

1. Introduction

The biosphere emits considerable amounts of biogenic volatile organic compounds (BVOCs), which have important impacts on atmospheric chemistry. Isoprene (C_5H_8) is the most abundant one, with global emissions estimated in the range 361 to 660 Tg C yr^{-1} (Arneth et al., 2008; Guenther et al., 2006; Müller et al., 2008). Once in the atmosphere, isoprene impacts the oxidative capacity of the troposphere due to its fast reactivity with major oxidants (Atkinson, 2000). Emissions originating from the ocean, estimated in the range 0.1–11.6 Tg C yr^{-1} (Arnold et al., 2009; Bonsang et al., 1992; Booge et al., 2016; Gantt et al., 2009; Hu et al., 2013; Luo & Yu, 2010; Palmer & Shaw, 2005; Sinha et al., 2007), are far less important than emissions by terrestrial plants and hence would result in a globally limited impact on atmospheric chemistry (Anttila et al., 2010; Arnold et al., 2009). However, as isoprene has a very short atmospheric lifetime (typically from minutes to hours), the marine boundary layer (MBL) over remote oceanic areas is not impacted by the strong terrestrial fluxes, but by direct oceanic emissions (Kameyama et al., 2014). Isoprene, being a precursor of secondary organic aerosols (SOAs) (Claeys, 2004; Kroll et al., 2006), could be involved in negative climate feedbacks as SOA contributes to the production of cloud condensation nuclei (CCN) (Carslaw et al., 2010). In the remote MBL, an abrupt increase of marine isoprene emissions would play a significant role in isoprene-derived SOA formation, especially during phytoplankton blooms (Hu et al., 2013; Meskhidze & Nenes, 2006; Myriokefalitakis et al., 2010).

The phytoplankton origin of marine isoprene was confirmed by a number of field measurements conducted since the early 1990s (Baker et al., 2000; Bonsang et al., 1992; Broadgate et al., 1997; Hackenberg et al., 2017; Kameyama et al., 2014; Kurihara et al., 2010; 2012, Matsunaga et al., 2002; Milne et al., 1995; Ooki et al., 2015; Shaw et al., 2003; Tran et al., 2013; Wingenter et al., 2004). During these campaigns, marine isoprene concentrations were shown to vary widely across locations and seasons, from less than 1 to 200 pmol L^{-1}. In

addition, the vertical distribution of isoprene in the upper ocean was observed to mainly follow chlorophyll-a (Chla) concentrations with the presence of subsurface maxima, suggesting a strong isoprene biogenic source. The rates of isoprene phytoplankton production were determined through laboratory experiments, which resulted in Chla-normalized phytoplankton production rates varying by more than two orders of magnitude (0.03 to 1.34 μmol C_5H_8 g $Chla^{-1}$ h^{-1}) (Bonsang et al., 2010; Exton et al., 2013; Gantt et al., 2009; McKay et al., 1996; Meskhidze et al., 2015; Moore et al., 1994; Shaw et al., 2003). This variability may be due to differences in production rates between major phytoplankton functional types (PFTs) (Booge et al., 2016; Colomb et al., 2008; Exton et al., 2013) or to differences in environmental forcing parameters such as temperature (Exton et al., 2013) and light (Bonsang et al., 2010; Gantt et al., 2009; Shaw et al., 2003). However, the large range of production rates inferred from the experimental studies makes it difficult to generalize these rates to all phytoplankton species or PFTs. Additionally, the precise mechanisms that are responsible for phytoplankton isoprene production are still unclear, and it is yet difficult to draw similarities with terrestrial plants for which isoprene production has been mainly related to protection against heat stress and reactive oxygen species (ROS; Sharkey & Monson, 2017; Sharkey & Yeh, 2001; Zeinali et al., 2016). The main loss of isoprene in the ocean is via air-sea gas exchange (Booge et al., 2018; Kameyama et al., 2014; Palmer & Shaw, 2005), but isoprene is also consumed in situ by biochemical processes. In particular, it is known that isoprene reacts in aqueous phase with major ROS (Palmer & Shaw, 2005; Riemer et al., 2000; Zinser, 2018), despite the fact that turnover times associated to these oxidations are highly uncertain. With two energy-rich double bonds, isoprene could also be readily consumed by diverse phyla of bacteria (Gray et al., 2015; Srivastva et al., 2017), as attested in terrestrial soils (Cleveland & Yavitt, 1997, 1998; El Khawand et al., 2016; Ewers et al., 1990; Van Ginkel et al., 1987) and freshwater sediments (Vlieg et al., 1998). Alvarez et al. (2009) and Johnston et al. (2017) demonstrated isoprene consumption in samples from marine and estuarine waters, but the importance of a biological consumption in the open ocean is still unconfirmed.

Large uncertainties regarding the quantification of marine isoprene emissions are also persistent. Bottom-up approaches, based on extrapolation of in situ observations or modeling of oceanic isoprene concentrations, give rise to estimates that range between 0.1 and 1.2 Tg C yr^{-1} (Arnold et al., 2009; Bonsang et al., 1992; Booge et al., 2016; Gantt et al., 2009; Palmer & Shaw, 2005; Sinha et al., 2007). Most of these bottom-up approaches used remote-sensing Chla concentrations to derive surface oceanic isoprene concentrations. To do so, they assumed steady state isoprene concentrations in the oceanic mixed layer. They either used a constant production rate of isoprene (Palmer & Shaw, 2005), or differentiated isoprene production for the main PFTs (Arnold et al., 2009; Booge et al., 2016) in combination with the PHYSAT algorithm to estimate PFT partitioning at the global scale (Alvain et al., 2005). Gantt et al. (2009), however, used a variable production rate as a function of the incoming photosynthetically active radiation (PAR). In parallel, top-down approaches have also been applied to estimate the global oceanic isoprene flux, constraining oceanic emissions with atmospheric concentrations measured in the MBL. Such approaches lead to global estimates in the range 1.5 to 11.6 Tg C yr^{-1} (Arnold et al., 2009; Hu et al., 2013; Luo & Yu, 2010), much higher than estimates from bottom-up approaches. A commonly mentioned process to explain these discrepancies is the direct emission of isoprene from the sea surface microlayer (SML), based on the studies of Ciuraru et al. (2015a, 2015b), that showed experimental evidences of isoprene photoproduction by surfactants in an organic monolayer at the air-sea interface. Very recently, Brüggemann et al. (2018) developed a parameterization of this interfacial photoproduction and estimated an isoprene flux from the SML to the atmosphere between 0.62 and 1.34 Tg C yr^{-1}.

Our objective here is to try to reconcile existing experimental, in situ, and theoretical knowledge of the marine isoprene cycle through the use of a global 3D oceanic biogeochemical model in combination with an original data set gathering in situ measurements of oceanic isoprene concentrations. To this end, we explore different plausible parameterizations of the oceanic isoprene sources and sinks, largely inspired from available laboratory experiments. We provide the first 3D global estimates of the oceanic isoprene cycle and a new spatiotemporal distribution of isoprene emissions to the atmosphere, which also includes a representation of the photoproduction occurring in the SML. Those new estimates are proposed for use in atmospheric chemistry models, to better appraise the importance of oceanic BVOCs on the MBL chemistry, as well as to investigate potential climate feedbacks. Finally, we identify specific gaps in our process understanding and potential inconsistencies between theoretical understanding, in situ observations, and laboratories experiments.

2. Materials and Methods

2.1. Collection of Experimental and In Situ Data

Isoprene production rates by phytoplankton measured in laboratory experiments were collected from the literature (Bonsang et al., 2010; Exton et al., 2013; Meskhidze et al., 2015; Shaw et al., 2003), for diverse marine phytoplankton cultures. Some experiments also attempted to investigate the separate effects of light (Bonsang et al., 2010; Shaw et al., 2003) and of temperature (Exton et al., 2013; Shaw et al., 2003), or their combined effects (Meskhidze et al., 2015) on production rates. In total, 95 rates were collected for all phytoplankton species combined and were used to help constraining the parameters of the isoprene module implemented in the Nucleus for European Modelling of the Ocean, Pelagic Interaction Scheme for Carbon and Ecosystem Studies (NEMO-PISCES) model presented hereafter.

Isoprene concentrations measured at sea were also collected from the literature. Two types of measurements were gathered: sea surface isoprene concentrations (typically from 5-m depth) as well as vertical profiles documenting isoprene concentrations as a function of depth (typically for the top 100 m). For the surface measurements, 13 individual data sets are used (Bonsang et al., 1992; Booge et al., 2016; Gros & Bonsang, 2019; Gros et al., 2019; Hackenberg et al., 2017; Matsunaga et al., 2002; Milne et al., 1995; Ooki et al., 2015; Tran et al., 2013). Their spatiotemporal coverage is rather poor (Figure 1). Most regions have been sampled only at a specific season, and some wide areas are not documented as in the Southern and Pacific oceans. To evaluate our model output, and because the model horizontal resolution used here is rather coarse, we averaged all observed data points located in a same $2° \times 2°$ grid cell, for the same month, the same year, and the same author. After processing, 572 surface data points are available.

Isoprene vertical profiles were retrieved from the AMT 22 and AMT 23 cruises (Hackenberg et al., 2017). Isoprene concentrations from these vertical profiles were also averaged on $2° \times 2°$ grid cells, as for the surface data, which resulted in 16 different vertical profiles, all located in the Atlantic Ocean. Chla concentrations estimated from fluorescence measurements during these campaigns (Hackenberg et al., 2017) were also retrieved. All Chla data have been averaged on $2° \times 2°$ grid cells and were selected where isoprene profiles are available for the same location and month. Location of these Chla and isoprene vertical profiles is shown on Figure 1.

2.2. Biogeochemical Model

We used the global ocean biogeochemistry model *Pelagic Interaction Scheme for Carbon and Ecosystem Studies* (PISCES) in its version 2 (described and evaluated in details in Aumont et al., 2015). We recall here its main characteristics. PISCES includes two phytoplankton types (nanophytoplankton and diatoms), two zooplankton size classes (microzooplankton and mesozooplankton), two organic particle size classes, and semilabile dissolved organic matter. Phytoplankton growth is limited by temperature, light, and by five nutrients (NO_3^-, NH_4^+, PO_4^{3-}, Si $(OH)_4$, and dissolved Fe). Mortality, aggregation, and grazing also influence the evolution of phytoplankton biomass. Chla concentrations for the two phytoplankton types are prognostically computed, using the photoadaptative model of Geider et al. (1996).

2.3. Isoprene Module

A specific module has been added to PISCES in order to explicitly represent the oceanic isoprene sources and sinks: phytoplankton production ($Prod_{Phyto}$), biochemical consumption ($Cons_{Biochem}$), and air-sea gas exchange ($Flux_{ocean}$). They affect the oceanic isoprene concentration according to

$$\frac{dISO}{dt} = Prod_{Phyto} - Cons_{Biochem} - Flux_{ocean.} \quad (1)$$

Note that isoprene concentrations are advected and diffused as any other passive tracer in PISCES.

An additional flux to the atmosphere ($Flux_{SML}$), corresponding to the direct emission of isoprene due to photoproduction occurring in the SML, is also represented. This flux does not impact the oceanic isoprene concentration and is thus not included in Equation 1.

2.3.1. Phytoplankton Production

Oceanic isoprene is produced by phytoplankton, and the production is usually parameterized as a function of Chla concentrations (Booge et al., 2016; Gantt et al., 2009; Palmer & Shaw, 2005). Based on this

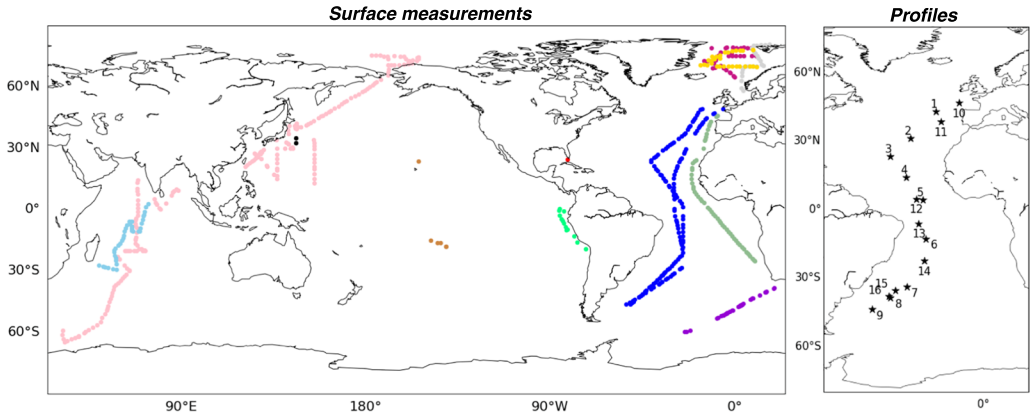

Surface measurements:		Number of data points
Bonsang et al., 1992	Data from different cruises (April 1990, May-June 1987). Data reported from Table 1	6
Booge et al., 2016	ANT-XXV/1 cruise, November 2008 (Seawater from approximately 2 m depth was continuously pumped on board)	54
Booge et al., 2016	ASTRA-OMZ cruise, October 2015 (Water samples taken every 3 h from a continuously running seawater pump system at approximately 6 m depth)	13
Booge et al., 2016	SPACES/OASIS cruises, June-July 2014 (Water samples taken every 3 h from a continuously running seawater pump system at approximately 6 m depth)	39
Gros and Bonsang 2019	OOMPH cruise, March 2007 (Water samples taken from a continuously running seawater pump system at approximately 8 m depth)	37
Gros et al., 2019	TRANSSIZ cruise, May 2015 (Water samples taken every 3 minutes from a continuously running seawater pump system at approximately 6 m depth)	24
Hackenberg et al., 2017	ACCACIA 1 cruise, March 2013 (measurements from underway seawater sampled at nominal depth 5–6 m)	30
Hackenberg et al., 2017	AMT22, October-November 2012 and AMT23, October-November 2013 (measurements from underway seawater sampled at nominal depth 5–6 m)	138
Matsunaga et al., 2002	R/V Mirai cruise, May 2001 (Surface seawater samples were collected from 10 m in water depth using Niskin bottles installed in a CTD system). Data reported from Table 1	2
Milne et al., 1995	September 1993, seawater samples taken at depth with CTD. Surface data reported from Table 1 and averaged	1
Ooki et al., 2015	Data from 7 cruises, covering different seasons from January 2008 to October 2012 (Surface mixed layer seawater was pumped at 5 m depth)	195
Tran et al., 2013	ARK XXV1+2 cruises, June-July 2010 (Water samples taken from a seawater pump system at 6 m depth)	33
Profiles:		**Number of profiles**
★ Hackenberg et al., 2017	AMT22, October/November 2012 (profiles 1-9) and AMT23, October/November 2013 (profiles 10-16), from CTD measurements.	16

Figure 1. Location of the isoprene concentration observations (surface data and vertical profiles) retrieved from the literature. Data are presented after post-treatment (averaging per 2° grid cells), and the mean position and the number of surface data points or number of profiles finally obtained are reported.

assumption, the phytoplankton production of isoprene (μmol C_5H_8 L^{-1} d^{-1}) is computed using the following relation:

$$Prod_{Phyto} = (p_{nano}Chla_{nano} + p_{diat}Chla_{diat}) \times h, \quad (2)$$

with $Chla_{nano}$ and $Chla_{diat}$ (in g Chla L^{-1}) being the respective Chla concentrations for nanophytoplankton and diatoms and p_{nano} and p_{diat} their respective Chla-normalized production rates in μmol C_5H_8 g $Chla^{-1}$ h^{-1}. To account for the variation of daylight, production is multiplied by the daylength h in hours computed as a function of latitude and period of the year. As some laboratory studies suggested an impact of temperature on the phytoplankton production of isoprene (Exton et al., 2013; Meskhidze et al., 2015;

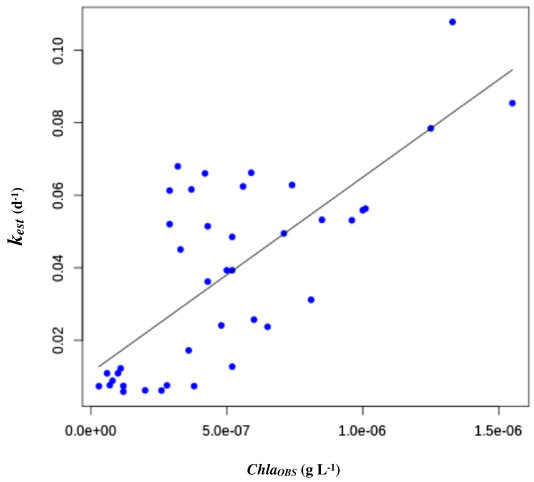

Figure 2. Scatter plot of estimated consumption rates ($k_{est.}$) versus observed Chla concentrations ($Chla_{OBS}$). Chla corresponds to measurements performed at different depths by fluorescence during the AMT 2012 cruise (Hackenberg et al., 2017). The correlation is statistically significant ($p < 0.05$, $n = 40$), with $R^2 = 0.54$.

Shaw et al., 2003), production rates p_{nano} and p_{diat} are computed as a function of the water temperature (T in °C). A linear relationship is assumed:

$$p_{nano} = \mu_{nano}[1 + \alpha(T - T_m)] \tag{3a}$$

$$p_{diat} = \mu_{diat}[1 + \alpha(T - T_m)]. \tag{3b}$$

Laboratory studies remain too scarce so far to be able to derive robust values for the parameters μ_{nano}, μ_{diat}, T_m, and α. They indicate, however, plausible ranges of values for the rates p_{nano} and p_{diat}. We conducted a series of sensitivity tests using a range of values for each of the parameter: 0.1–1.0 μmol C_5H_8 g Chla^{-1} h^{-1} for μ_{nano} and μ_{diat}, 13–20°C for T_m, and 0.02–0.1 for α. After each sensitivity test, we performed a comparison of the simulated isoprene surface concentrations to the observed ones and a comparison of the resulting rates p_{nano} and p_{diat} to the ones retrieved from laboratory experiments. In order to minimize the model-data differences, we fixed the parameter values at 0.45 μmol C_5H_8 g Chla^{-1} h^{-1} for μ_{nano}, 0.25 μmol C_5H_8 g Chla^{-1} h^{-1} for μ_{diat}, 16.5°C for T_m, and 0.05 for a.

2.3.2. Biochemical Consumption

Due to the large uncertainties regarding isoprene biochemical consumption, we adopt here a simple parameterization. We consider that the biochemical loss of isoprene in the ocean follows first-order kinetics and as such is proportional to isoprene concentration:

$$Cons_{Biochem} = k_{tot} \times ISO, \tag{4}$$

with k_{tot} the total loss rate (in d^{-1}). This rate includes the chemical loss due to the reaction of isoprene in aqueous phase with major ROS, such as the hydroxyl radical (OH) and the singlet oxygen ($^1O_2$) (Palmer & Shaw, 2005), and the bacterial consumption (Booge et al., 2016; Palmer & Shaw, 2005).

To constrain the value of k_{tot}, we made use of the vertical profiles collected during the AMT 2012 cruise (Hackenberg et al., 2017). Below a certain depth, exchanges of isoprene with the atmosphere are negligible and subsurface isoprene concentrations result from an equilibrium between production and consumption. An analysis of the retrieved vertical profiles showed that 20 m is a reasonable depth, as measured isoprene concentrations generally exhibit a (positive) gradient below that depth. Hence, a consumption rate $k_{est.}$ is estimated from each pair i of isoprene (ISO_{OBS}) and Chla ($Chla_{OBS}$) measured below 20 m:

$$k_{est._i} = P \times \left.\frac{Chla_{OBS}}{ISO_{OBS}}\right|_i \tag{5}$$

with P the isoprene production rate, taken as 0.185 μmol C_5H_8 g Chla^{-1} h^{-1}, which corresponds to the mean value of the isoprene production rates measured in laboratory experiments, all species combined. Then, a linear regression is performed between $k_{est.}$ and $Chla_{OBS}$ (Figure 2) based on the following equation:

$$k_{est._i} = \mu Chla_{OBS_i} + k_{Chem} \tag{6}$$

This results in a significant correlation ($p < 0.05$, $n = 40$), with a coefficient of regression R^2 of 0.54. The retrieved slope μ is equal to 53,850 (g Chla L^{-1})$^{-1}$ d^{-1}, and the retrieved intercept, noted k_{Chem}, is equal to 0.01 d^{-1}. From this, k_{tot} is modeled in NEMO-PISCES as

$$k_{tot} = \mu(Chla_{nano} + Chla_{diat}) + k_{Chem}. \tag{7}$$

The constant part is assumed to be the chemical loss. The variable part is assumed to represent the bacterial consumption of isoprene, with a rate k_{Bio} introduced such as

$$k_{Bio} = \mu(Chla_{nano} + Chla_{diat}). \quad (8)$$

2.3.3. Ocean-Atmosphere Exchanges

The total isoprene flux at the ocean-atmosphere interface ($Flux_{tot}$) is described as the sum of the oceanic isoprene flux ($Flux_{ocean}$), that is, the flux due to the isoprene pool produced and consumed in the water column, and of the SML flux ($Flux_{SML}$), that is, the flux due to the interfacial photolysis of SML surfactants:

$$Flux_{tot} = Flux_{ocean} + Flux_{SML.} \quad (9)$$

The oceanic isoprene flux $Flux_{ocean}$ to the atmosphere is described in a similar way to the Fick's diffusion law. It depends on the concentration at the ocean surface and on the partial pressure in the atmosphere above the ocean ($pISO_a$ in atm):

$$Flux_{ocean} = k_{flx}(ISO - H \times pISO_a) \quad (10)$$

$$pISO_a = p_{atm} \times f_{ISO} \quad (11)$$

with p_{atm} the atmospheric pressure and f_{ISO} the atmospheric dry molar fraction of isoprene. H is the Henry's law constant, which relates the partial pressure of a gas with the equilibrium concentration in solution (ISO^*):

$$ISO^* = H \times pISO_a. \quad (12)$$

It is calculated from Mochalski et al. (2011) by

$$H = exp\left[-17.85 + \frac{4130}{T + 273.16}\right] \times 100. \quad (13)$$

Finally, k_{flx} is the gas transfer velocity (in m s^{-1}). It depends on the wind speed at 10-m height (u in m s^{-1}) according to the Wanninkhof (1992) parameterization and on the Schmidt number (sch, dimensionless), described as a quadratic function of the seawater temperature (Tran et al., 2013).

$$k_{flx} = \left[0,251u^2\right] \times \left[\frac{660}{sch}\right]^{1/2} \quad (14)$$

In order to maximize the flux of isoprene emitted to the atmosphere, the atmospheric dry mole fraction f_{ISO} is taken equal to zero. Over the open ocean, because of the short atmospheric lifetime of isoprene, this assumption might be justified. However, over the coastal ocean, this assumption may not be valid because of the strong terrestrial plant inputs.

The SML isoprene flux is computed based on the parameterization of Brüggemann et al. (2018). It is described as the photochemical emission potential (μ_{photo} in mW m^{-2}) multiplied by the photochemical isoprene flux from the marine SML and biofilm measured in laboratory studies (F_{lab} in molecules of isoprene mW^{-1} s^{-1}):

$$Flux_{SML} = F_{lab} \times \mu_{photo}. \quad (15)$$

Previously reported values for F_{lab} vary between 3.71 and 6.19 × 10^7 molecules mW^{-1} s^{-1} (Brüggemann et al., 2017; Ciuraru et al., 2015a, 2015b). In PISCES, F_{lab} is set to 4.95 × 10^7 molecules mW^{-1} s^{-1}, corresponding to the mean value computed from the minimum and the maximum of this range. The emission potential μ_{photo} is described as a linear relationship of the ultraviolet solar radiation between 280 and 400 nm reaching the surface ocean ($E_{280–400}$ in mW m^{-2}):

$$\mu_{photo} = E_{280-400} \times F_{surf} \times k_{SML}. \quad (16)$$

In PISCES, $E_{280–400}$ is assumed to be 3.535% of the total solar irradiance. This fraction has been determined from the standard solar spectrum ASTM G173–03 (2012), modeled using the ground-based solar spectral irradiance SMARTS2 (version 2.9.2) *Simple Model for Atmospheric Transmission of Sunshine*. The correction factor F_{surf} accounts for variations of the surfactant concentrations in the SML. Following Brüggemann et al. (2018), it is expressed as

$$F_{surf} = \frac{ln(c_{surf})}{ln(c_{max,\,surf})} \tag{17}$$

with the surfactant concentration c_{surf} in the SML (in concentration equivalents of Triton X), calculated according to the method of Wurl et al. (2011). For oligotrophic waters with net primary production (NPP) < 0.4 g C m^{-2} d^{-1}, c_{surf} = 320 μg Teq L^{-1}. For eutrophic waters with NPP > 1.2 g C m^{-2} d^{-1}, c_{surf} = 663 μg Teq L^{-1}. For mesotrophic waters with NPP between 0.4 and 1.2 g C m^{-2} d^{-1}, c_{surf} = 502 μg Teq L^{-1}. In PISCES, no variations of $c_{surf,max}$ are considered and this concentration is set to its maximum proposed value, that is, 663 μg Teq L^{-1}. The factor k_{SML} allows to account for changes in the gas transfer velocity across the air-sea interface. As described in Brüggemann et al. (2018), it depends on the wind speed according to the parameterization of McGillis et al. (2004), and it is normalized to laboratory conditions of Ciuraru et al. (2015a) and Brüggemann et al. (2017):

$$k_{SML} = \frac{8.2 + [0.014 \times u^3]}{8.2 + [0.014 \times {u_{lab}}^3]} \tag{18}$$

with $u_{lab} = 5.31\times 10^{-2}$ m s^{-1}. Finally, the concentration of surfactant in the SML is considered significant and hence photochemically active only when the wind speed is below 13 m s^{-1} (Brüggemann et al., 2018). Above this threshold, the SML is considered unstable and free of surfactant.

2.4. Experiments

2.4.1. Standard Experiment

PISCES, including the isoprene module described above, is used in an offline configuration, that is, a climatological ocean dynamical state is first obtained from a NEMO physics-only simulation (version 3.6, Madec, 2008) and is then used when running PISCES. This physics-only simulation was obtained after a spin up of 200 years, starting from the climatology of Conkright et al. (2002) for temperature and salinity. It is forced by daily climatological atmospheric fields (air temperature, winds, precipitations, shortwave fluxes, etc.) and monthly precipitations, which were built from various data sets including the daily NCEP reanalysis (see Aumont et al., 2015 for details). The last year of the physics-only simulation (ocean currents, temperature, salinity, mixed layer depth, surface radiation, etc.) at 5-day temporal mean resolution is used to force PISCES. For all biogeochemical tracers except isoprene, PISCES is initialized after a 3,000-year long spin-up as detailed in Aumont et al. (2015). PISCES, including the isoprene module, is then run for two additional years. Only the second year is used for the study of the oceanic isoprene cycle, the first year being considered as a short spin-up which is sufficient because of the short lifetime of isoprene in the ocean (from a few days to a few weeks).

PISCES is here used within the global configuration ORCA2, whose spatial grid has a nominal horizontal resolution of 2° with 30 levels on the vertical dimension (10-m resolution in the first 200 m). In order to map the oceanic isoprene dynamic and to evaluate the concentrations against the in situ data set previously described, the model outputs have been regridded on a regular 2° × 2° grid, using a bilinear interpolation.

2.4.2. Sensitivity Experiments

The isoprene module described above is used to perform a first simulation, referred to here as the standard simulation (hereafter STD). Building from the STD simulation, we performed a series of four other simulations with the same experimental design, but with modifications in the way isoprene sources and sinks are parameterized. Each of those simulations is then compared with STD in order to evaluate the sensitivity of the isoprene concentrations and emissions to each process and/or its representation.

2.4.2.1. Simulation STD-PFT

This simulation aims to evaluate the relevance of differentiating the isoprene production between the two PFTs: nanophytoplankton and diatoms. In STD-PFT, the temperature-dependent rates p_{nano} and p_{diat}

(Equation 2) are kept the same by fixing the rates μ_{nano} and μ_{diat} (Equations 3a and 3b) at the same value, 0.35 μmol C_5H_8 g $Chla^{-1}$ h^{-1} (mean value between the rates μ_{nano} are μ_{diat} used in STD).

2.4.2.2. Simulation STD-T

Here, the importance of temperature as a driver of isoprene production is evaluated. To do so, the temperature dependence of the production rates is canceled and the rates p_{nano} and p_{diat} (Equation 2) are imposed constant with values corresponding to the average rates retrieved from laboratory experiments: 0.20 and 0.17 μmol C_5H_8 g $Chla^{-1}$ h^{-1} for nanophytoplankton and diatoms, respectively.

2.4.2.3. Simulation STD+I

Light intensity experienced by phytoplankton could influence isoprene production (Bonsang et al., 2010; Gantt et al., 2009; Shaw et al., 2003). We tested a light-dependent production, in addition to the temperature dependence. To link irradiance I (in μE m^{-2} s^{-1}) to isoprene production, we use the log relation of Gantt et al. (2009). Equations 3a and 3b become respectively

$$p_{nano} = \mu_{nano}[1 + \alpha(T - T_m)]\frac{ln(I)^2}{ln(I_m)^2} \tag{19a}$$

$$p_{diat} = \mu_{diat}[1 + \alpha(T - T_m)]\frac{ln(I)^2}{ln(I_m)^2}. \tag{19b}$$

The parameter I_m is fixed to 22.5 μE m^{-2} s^{-1}. Note that irradiance is considered here as the photosynthetic available radiation (PAR). To convert PAR, described in PISCES in W m^{-2} into units of μE m^{-2} s^{-1}, we use the following approximate conversion: 1 W m^{-2} ≈ 4.5 μE m^{-2} s^{-1}. The vertical penetration of PAR is described in details in Aumont et al. (2015).

2.4.2.4. Simulation STD-Chla

Here, we explore the relevance of using a variable isoprene consumption rate with Chla. In this simulation, the consumption term is simplified by keeping the bacterial rate k_{Bio} constant (equal to 0.01 d^{-1}, based on the study of Booge et al., 2016). The chemical rate k_{Chem} remains unchanged (0.01 d^{-1}), and hence, Equation 4) is used with a fixed k_{tot} of 0.02 d^{-1}.

3. Evaluation of the Standard Experiment

The STD simulation, in which the phytoplankton isoprene production depends on temperature and in which the consumption depends on Chla, is here evaluated against experimental and in situ measurements. For the comparison with in situ data, the simulated concentrations collocated in time (month of measurement) and space (2° × 2° cell) with the mean observed measurements were extracted from the model output. It is worth mentioning that this evaluation might be limited by the fact that the model is forced by climatological boundary conditions (temperature, winds, precipitation, etc.) and hence does not represent interannual variations of both the ocean dynamics and biogeochemistry.

3.1. Surface Concentrations

In the global ocean, simulated isoprene concentrations in the surface ocean (taken as the first 10-m depth) range from 0.6 to 52.7 pmol L^{-1}, with a mean value of 18.0 pmol L^{-1} for the months and locations collocated with observations. This range is lower than the range of observations for which upper values exceed 115.0 pmol L^{-1}. However, 75% of the observed concentrations are below 30.5 pmol L^{-1}, and the mean value is 21.8 pmol L^{-1}. Globally, 67% of the surface observations are represented within a factor of two by the model, and the corresponding root mean square error (RMSE) value is 14.5 pmol L^{-1} (Figure 3a). Figure 3b presents the zonally averaged simulated concentrations (annual mean and monthly maximum and minimum), as well as maximum and minimum monthly values across all longitudes. They are compared with observed concentrations at a specific month and location, according to their latitude. Simulated isoprene concentrations are high at the equator (averaged zonal mean value is 35 pmol L^{-1}), lower in the subtropical gyres (reduced to 10–15 pmol L^{-1}), and slightly higher again between 30° to 40° (at 20–25 pmol L^{-1}). This distribution is globally in agreement with the observations and in particular

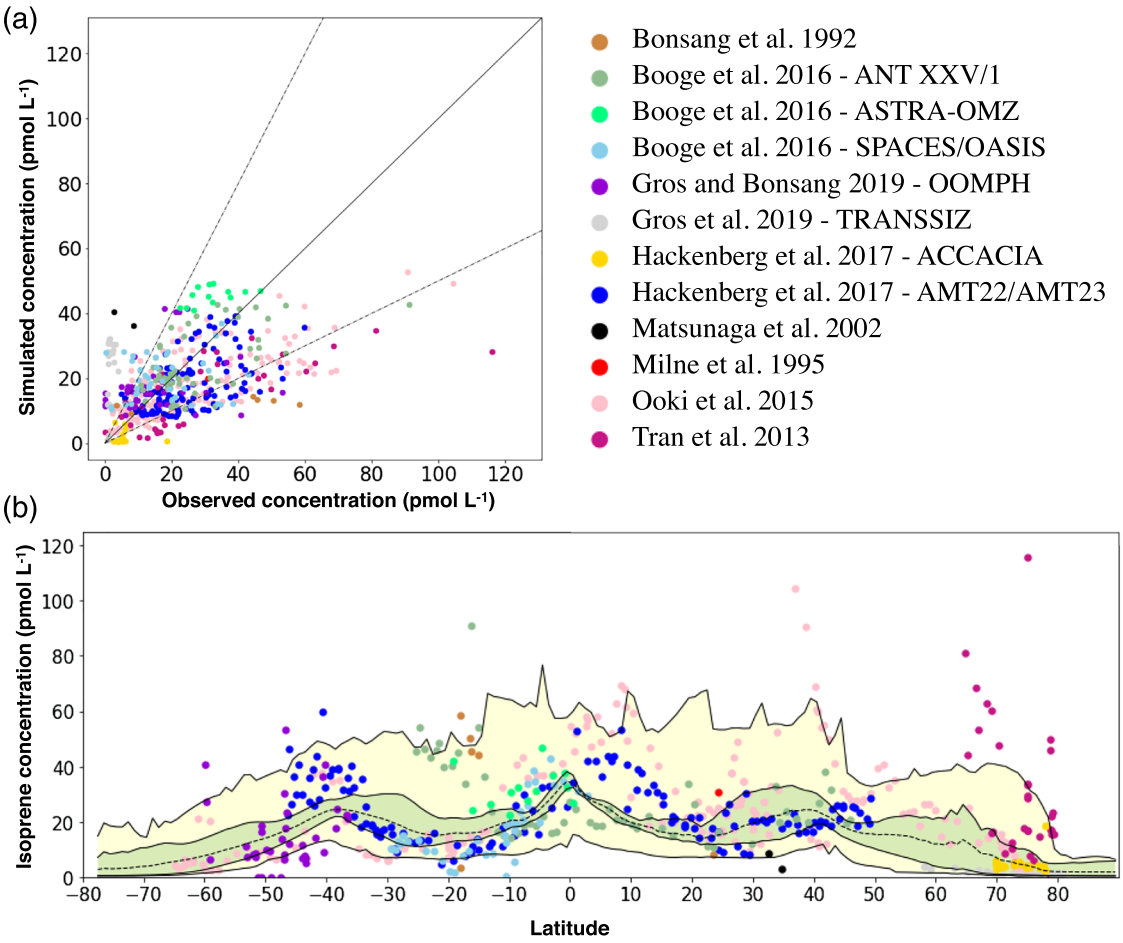

Figure 3. Comparison between simulated and observed isoprene concentrations in the surface ocean for the standard experiment. (a) Comparison using a scatter plot (the solid line represents the 1–1 line and dotted lines the 1–2 and 2–1 lines). (b) Surface concentrations as a function of the latitude (dots: observed concentrations; dotted line: longitudinal and monthly mean simulated isoprene concentration; green area: interval between maximum and minimum longitudinal mean concentrations; yellow area: interval between maximum and minimum concentrations at a given latitude).

with the data collected during the AMT 22 and AMT 23 cruises (Hackenberg et al., 2017) and with the data of Ooki et al. (2015), which cover a broad range of latitudes in the Atlantic, Pacific, and Indian Oceans. This distribution resembles that of Chla and has been interpreted as a signature of the biogenic origin of isoprene (Ooki et al., 2015). That said, the model underestimates isoprene concentrations in the Indian Ocean between 0° and 10° (Ooki et al., 2015) and also underestimates the concentrations measured by Bonsang et al. (1992) in April 1990 and May/June 1987 in the central Pacific. The lowest concentrations (<10 pmol L^{-1}) have been observed at latitudes higher than 50°, in particular by Ooki et al. (2015), Tran et al. (2013), Hackenberg et al. (2017), and Gros et al. (2019), but only a few observations are available, especially in the Southern Ocean. In these areas, the model also simulates low isoprene concentrations, due to low seawater temperature that strongly limits isoprene production. In the Arctic and sub-Arctic Oceans, the model accurately represents the data measured by Ooki et al. (2015) in the Pacific sector during September/October 2012 and the low concentrations measured in the Atlantic sector in March 2013 (Hackenberg et al., 2017). However, the model fails to reproduce the high isoprene concentrations measured by Tran et al. (2013) in June/July 2010, in particular concentrations exceeding 40 pmol L^{-1}.

3.2. Vertical Profiles

Figure 4 shows the simulated vertical profiles of isoprene concentrations (solid black line), collocated in time and space with the profiles retrieved from the AMT 22 and AMT 23 cruises after the averaging treatment (dashed black line). For a few observed profiles, isoprene concentrations stay relatively constant with

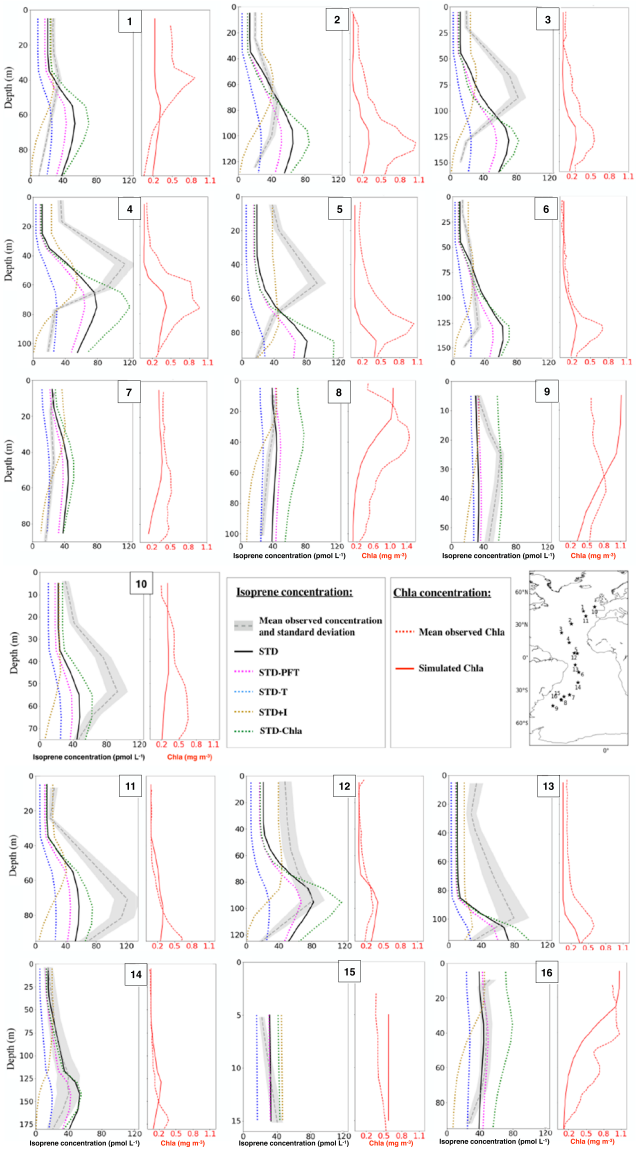

Figure 4. Comparison of oceanic isoprene profiles simulated with PISCES for different experiences with the measured profiles during AMT22 (profiles 1–9) and AMT23 (profiles 10–16) cruises. For each isoprene profile, the Chla measured during the same cruises by fluorescence (for the same month and location) is shown, as well as the Chla simulated with PISCES.

depth and lower than 50 pmol L^{-1} (see in particular the profiles n°7–8, 15–16, located between 30 and 40°S). Such profiles are accurately simulated (except an overestimation of about 20 pmol L^{-1} for the profile n° 7). Most observed profiles, however, present a subsurface maximum (see profiles n°2–5, 10–14), which can exceed 100 pmol L^{-1}. PISCES similarly simulates a maximum in the subsurface. For the AMT 22 profiles, this maximum is represented with a correct intensity, but is located deeper than the observed ones by about 15 to 30 m (see in particular n°2–5). For most of the AMT 23 profiles, isoprene concentrations at the subsurface maximum are underestimated, but the maximum is generally located at the same depth as the observed maximum (see in particular n°11, 12, and 14). In Figure 4, observed Chla vertical profiles are also depicted, as isoprene concentrations are assumed to be driven at first order by Chla because of its phytoplanktonic origin. Observed Chla concentrations are often poorly represented by PISCES for the selected months and locations, which makes it difficult to relate the Chla and isoprene discrepancies. Nevertheless, it can be mentioned that for a few profiles, the observed isoprene maximum is located above the observed Chla subsurface maximum (see the n°2–5 and 11). For those later profiles, however, the simulated isoprene maximum is located at the same depth as the simulated Chla. This biased location of the isoprene maximum points out that some biochemical processes controlling the isoprene concentration, or vertical mixing, might not be well represented.

3.3. Isoprene Production Rates

In the first 200 m, the mean simulated phytoplankton production rates are 0.35 μmol C_5H_8 g $Chla^{-1}$ h^{-1} (standard deviation is 0.23 μmol C_5H_8 g $Chla^{-1}$ h^{-1}) and 0.20 μmol C_5H_8 g $Chla^{-1}$ h^{-1} (standard deviation is 0.13 μmol C_5H_8 g $Chla^{-1}$ h^{-1}) for diatoms and nanophytoplankton, respectively. These simulated temperature-dependent production rates are in the range of values measured in controlled laboratory experiments for a variety of phytoplanktonic species: 0.03 to 1.34 μmol C_5H_8 g $Chla^{-1}$ h^{-1} for nanophytoplankton (mean is 0.20 μmol C_5H_8 g $Chla^{-1}$ h^{-1}) and from 0.03 to 0.39 μmol C_5H_8 g $Chla^{-1}$ h^{-1} (mean is 0.17 μmol C_5H_8 g $Chla^{-1}$ h^{-1}) for diatoms (Bonsang et al., 2010; Exton et al., 2013; Meskhidze et al., 2015; Shaw et al., 2003).

To conclude, the model simulates isoprene concentrations that are in broad agreement with the available observations. However, it does not successfully reproduce the vertical profiles retrieved from the AMT 22 and AMT 23 cruises. The vertical profiles of Chla concentration (assumed to drive isoprene concentrations) are also not well reproduced by the model for those specific months and locations, which complicates the evaluation of the vertical profiles.

4. Sensitivity Experiments

In this section, each sensitivity experiment is compared with the standard experiment (STD), in terms of skill to reproduce observed surface isoprene concentrations and vertical profiles. The importance of each process is then discussed.

4.1. Importance of Differentiating the Production by Distinct PFTs

The importance of separating the production of isoprene into different PFTs is here evaluated through the analysis of the STD-PFT experiment, in which isoprene production rates are the same for both nanophytoplankton and diatoms. The model solution is slightly modified from STD to STD-PFT. In the surface ocean,

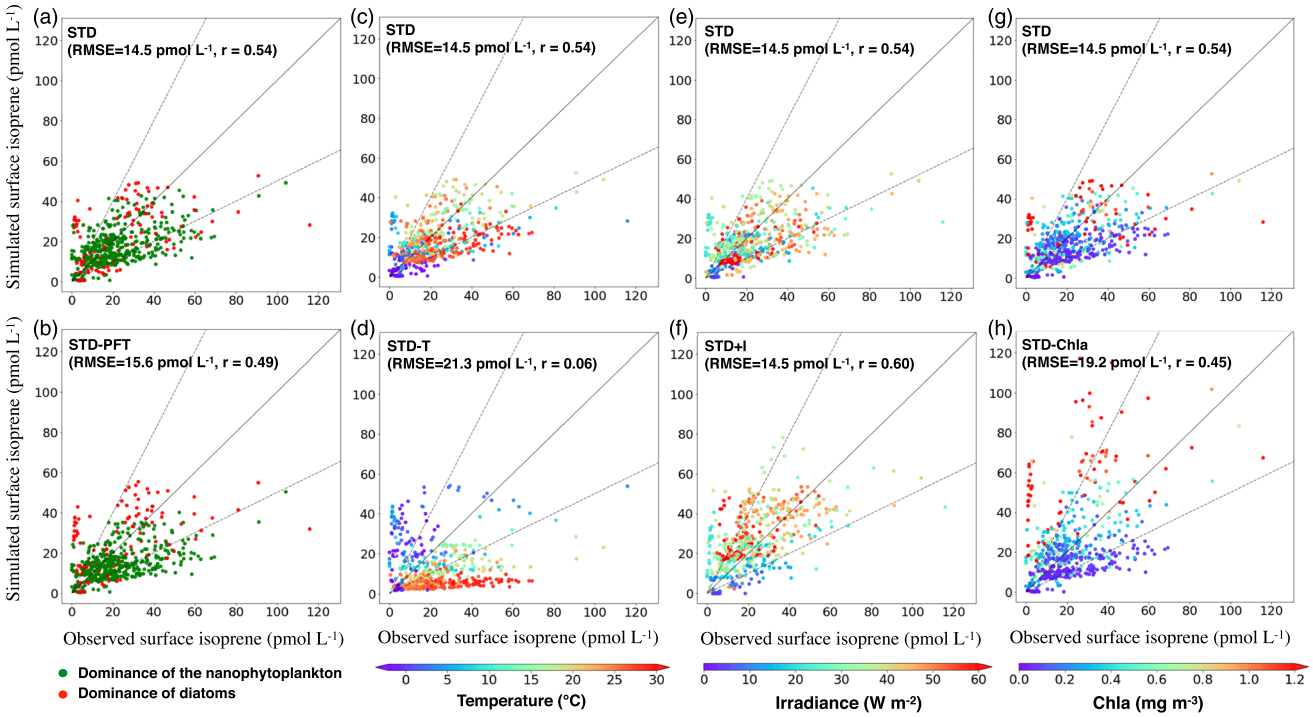

Figure 5. Comparison between simulated and observed isoprene concentrations in the surface ocean for the different simulations. Plots (a), (c), (e), and (g) for STD; (b) for STD-PFT; (d) for STD-T; (f) for STD+I; and (h) for STD-Chla. In plots (a) and (b), colors correspond to the dominance of the phytoplankton group. In (c) and (d), color varies with the temperature. In (e) and (f), color varies with the irradiance. In (g) and (h), color varies with Chla. The solid line represents the 1–1 line and dotted lines the 1–2 and 2–1 lines. For each simulation, the RMSE value and coefficient of correlation *r* between observed and simulated concentrations are mentioned.

the representation of isoprene concentrations is slightly degraded, with an RMSE value of 15.6 pmol L^{-1} for STD-PFT against 14.5 pmol L^{-1} for STD (Figures 5a and 5b). Below the surface, the shape of the isoprene vertical profile resulting from STD-PFT (Figure 4, dotted pink line) is similar to the one derived from STD. Quantitatively, concentrations are reduced for a few profiles, especially for the ones located at low latitudes (see profiles n°4–6 and 12–13). This decrease, of about 10 pmol L^{-1} at most, is explained by the dominance of nanophytoplankton at low latitudes (Alvain et al., 2005). Indeed, the mean production rate μ_{nano} is decreased from 0.45 μmol C_5H_8 g $Chla^{-1}$ h^{-1} in STD to 0.35 μmol C_5H_8 g $Chla^{-1}$ h^{-1} in STD-PFT.

The limited changes between STD-PFT and STD indicate that introducing two PFTs in the model, which have production rates of the same order of magnitude, is not particularly relevant to better simulate isoprene concentrations. However, this analysis is limited by the small number of PFTs (only two) represented in PISCES, especially considering the huge diversity of species included in the very generic nanophytoplankton group of PISCES. Variations of the production rate have previously been reported across four main PFTs: diatoms, *Synechococcus*, *Prochlorococcus*, and haptophytes (Bonsang et al., 2010; Booge et al., 2016; Exton et al., 2013; Tran et al., 2013). To predict oceanic isoprene, phytoplankton isoprene production was separated into at least those four main groups by some previous modeling studies (Arnold et al., 2009; Booge et al., 2016; Gantt et al., 2009), in combination with their respective Chla proportions retrieved from satellite observation and the use of algorithms such as PHYSAT (Alvain et al., 2005). However, there is still a large variability among the experimental rates available in the literature, even within one PFT. Indeed, among the experimental data available in the literature, we found a range of 0.100–0.490 μmol C_5H_8 g $Chla^{-1}$ h^{-1} for *Synechococcus* ($n = 3$ values), a unique value of 0.107 μmol C_5H_8 g $Chla^{-1}$ h^{-1} for *Prochlorococcus*, a range of 0.071–0.640 μmol C_5H_8 g $Chla^{-1}$ h^{-1} for haptophytes ($n = 9$ values), and a range of 0.030–0.390 μmol C_5H_8 g $Chla^{-1}$ h^{-1} for diatoms ($n = 61$ values). We do think that there are differences in the ability to produce isoprene among species, as it is the case for terrestrial plants (Arneth et al., 2007). However, as pointed

out by Booge et al. (2018), part of this variability could be attributed to differences in forcing environmental conditions for which species have been acclimated to.

4.2. Importance of the Temperature Dependence

The influence of temperature on the isoprene production rate is evaluated here by comparing STD-T and STD experiments. In the surface ocean, the representation of isoprene concentrations is largely degraded when the temperature dependence is suppressed. Indeed, the RMSE value is 21.3 pmol L^{-1} in STD-T against 14.5 pmol L^{-1} in STD. Figures 5c and 5d show the dispersion between collocated observed and simulated surface concentrations for both simulations, as a function of surface oceanic temperature. In STD-T, the differences between the observed and simulated concentrations present a strong correlation with temperature. STD-T results in a strong overestimation of most data points where surface temperature is below 10°C. Indeed, the model overestimates isoprene concentrations by more than a factor of two in the Atlantic sector of the Arctic (Tran et al., 2013) and in the Bering Sea (Ooki et al., 2015). In contrast, where surface temperatures exceed 20°C, most simulated isoprene concentrations are largely underestimated in STD-T. This is the case for example for the data collected during the AMT 22 and AMT 23 cruises (Hackenberg et al., 2017), for the data of Bonsang et al. (1992) collected in the central Pacific, or for the data collected in the Atlantic and in the Indian Ocean (Booge et al., 2016). In the subsurface, the vertical isoprene profiles from STD-T (Figure 4, dotted blue line) are very similar to the ones from STD, with slightly lower values. The difference between STD and STD-T is the largest for vertical profiles located at low latitudes (by up to 50 pmol L^{-1} at depth where the maximum of isoprene is found; see profiles 4–5 and 12–13). This is expected as isoprene production in relatively warm waters is no more enhanced by temperature in STD-T.

Our results highlight the sensitivity of isoprene concentrations to variability in water temperature. The processes by which temperature influences phytoplankton isoprene production are still poorly understood. Some laboratory studies have suggested a direct impact of temperature on isoprene production by marine phytoplankton. Exton et al. (2013) found a positive correlation for some Bacillariophyceae and Dinophyceae species (classes of diatoms), and Shaw et al. (2003) showed that isoprene production is maximum at about 23°C for *Prochlorococcus*. Meskhidze et al. (2015) have investigated two diatoms species: *Thalassiosira weissflogii* and *Thalassiosira pseudonana* and also found a significant temperature dependence. However, there are too few studies conducted, and overall too few species investigated, to be able to derive robust parameterizations from laboratory experiments. Recently, Ooki et al. (2015) and Hackenberg et al. (2017) have analyzed data sets of in situ surface isoprene concentrations covering a large range of latitudes and have pointed out the importance of temperature in driving oceanic isoprene concentrations. They calculated linear regressions between isoprene and Chla concentrations and found significant coefficients of correlation when splitting by different ranges of sea surface temperature.

It is worth mentioning some important metabolic and functional aspects of isoprene production by terrestrial plants that have been shown to be linked to temperature, even though this cannot be directly extrapolated to the marine realm. It is known that isoprene synthesis is performed through the methylerythritol 4-phosphate (MEP) metabolic pathway (Dani & Loreto, 2017; Lohr et al., 2012; Schwender et al., 1996), the same one that produces many other compounds such as other BVOCs, carotenoids, and hormones (Lichtenthaler, 2009; Loreto & Fineschi, 2015). This pathway is present in many bacteria and photosynthetic organisms (Lichtenthaler et al., 1997) and is ubiquitous in marine phytoplankton (Lohr et al., 2012). It occurs in chloroplasts and uses carbon compounds directly from the Calvin cycle of the photosynthesis (Ferrieri et al., 2005; Schnitzler, 2004; Sharkey & Monson, 2017). Two main hypotheses are put forward to explain the benefits of isoprene production for terrestrial plants facing temperature changes. The first hypothesis relates to the role of isoprene production in getting rid of excess carbon and energy produced during active photosynthesis (Logan et al., 2000; Pollastri et al., 2014; Sanadze, 2004; Sharkey et al., 2008), as there is a strong influence of temperature on enzymatic reactions in general and on those catalyzing isoprene (Loreto & Schnitzler, 2010). The second one is a role of thermoprotection, with isoprene stabilizing membranes during stressing temperature events (Sharkey & Yeh, 2001). However, unlike the energy dissipation hypothesis, the response to a thermal stress could be less relevant to explain marine isoprene production (Meskhidze et al., 2015; Shaw et al., 2003) as phytoplankton are usually exposed to more stable temperatures in the ocean.

Considering the different arguments mentioned above, we do think that a direct relation between isoprene production by oceanic phytoplankton and temperature exists. However, it is important to point out that the covariations we observed between temperature and isoprene concentrations could also be a consequence of other variables influencing isoprene production, which would covary with temperature at the scale of the global ocean. An example of such a case is phytoplankton speciation with latitude. Cyanobacteria, in particular *Synechococcus*, dominate at low latitudes (Alvain et al., 2005; Flombaum et al., 2013), whereas diatoms and haptophytes dominate at high latitudes (Alvain et al., 2005; Ben Mustapha et al., 2014). If isoprene production is closely linked to PFTs and that warm water species produce more isoprene than cold water species, then speciation could explain at least part of the observed pattern with temperature, as already mentioned by Hackenberg et al. (2017). The analysis of laboratory-retrieved isoprene production rates shows that the mean estimated rate of *Synechococcus* (0.335 μmol C_5H_8 g $Chla^{-1}$ h^{-1}) is higher than the mean of other groups (0.107 μmol C_5H_8 g $Chla^{-1}$ h^{-1} for *Prochlorococcus*, 0.192 μmol C_5H_8 g $Chla^{-1}$ h^{-1} for haptophytes, and 0.169 μmol C_5H_8 g $Chla^{-1}$ h^{-1} for diatoms), which supports such influence. This mean is however based on only three estimates, and the trend is only observable for this group.

4.3. Importance of the Light Dependence

The importance of light for producing isoprene is here evaluated with the STD+I experiment, in which p_{nano} and p_{diat} are both dependent on temperature and light. Figures 5e and 5f show the differences between observed and simulated surface concentrations as a function of the simulated irradiance in the surface layer of the ocean. RMSE value is unchanged compared with the STD experiment (14.5 pmol L^{-1}). Additionally, there is no clear pattern between simulated biases and light levels, for both simulations. Below the surface, isoprene profiles are however strongly modified in STD+I (Figure 4, dotted yellow line). For all profiles, light stimulates isoprene production in the surface ocean, resulting in increased surface concentrations of about 0 to 20 pmol L^{-1}. In contrast, concentrations are highly reduced below 60 m, by about 30 to 60 pmol L^{-1}. At these depths, light is strongly attenuated and hence limits isoprene production in the case of light dependence. Additionally, the STD+I experiment leads to isoprene maxima located further up in the water column. This helps representing the location of the observed isoprene maxima for the AMT 22 profiles (see profiles n°2–5), especially where observed maxima are located above the corresponding Chla maxima. Nevertheless, for profiles 2 and 3, maxima are now located about 20 m shallower than the observed ones, and for profiles n°3–5, their intensity is highly underestimated (by about 60 pmol L^{-1}). For the AMT 23 profiles, the STD+I experiment produces isoprene profiles that are not in agreement with the observed ones, especially because of too low concentrations at depth.

At the surface, our results show a limited impact of light on isoprene concentrations. Light dependence produces a decoupling between isoprene and Chla profiles with depth. This effect could be relevant to explain why the isoprene maximum is located shallower than the Chla maximum in some profiles. Nevertheless, the light dependence produces too low isoprene concentrations below the subsurface maximum for a majority of the available profiles.

As for temperature, the knowledge about the link between light and isoprene production by marine phytoplankton is still poor. Some laboratory studies have investigated the influence of light variations (taken as PAR radiation) on isoprene production rates, whereas Bonsang et al. (2010) found a relation only for a few diatom species, Shaw et al. (2003) found a relation for *Prochlorococcus*, and Gantt et al. (2009) for cyanobacteria, diatoms, and coccolithophores. For terrestrial plants, a relationship between isoprene emission and PAR light has been evidenced (Sharkey et al., 1995; Tingey et al., 1991) and was shown to be similar to that of photosynthesis (Guenther et al., 1991; Sharkey & Monson, 2017), with a link with the photosynthetic electron transport system (Sharkey & Monson, 2017). However, it is not known whether isoprene could have a direct functional role linked to PAR levels, but it could have a direct protection role for cell membranes facing oxidative damages caused by UV radiations (Loreto & Schnitzler, 2010).

Here, it is difficult to settle whether light is an important driver of marine isoprene production. Considering first the very limited importance of light for the evaluation of the isoprene surface concentrations, and second the fact that light strongly modifies the shape of the vertical profiles towards a strong decoupling between isoprene and Chla, we chose not to keep this parameter into the calculation of the production. However, light partly helps to represent a shift in the location between the isoprene and Chla maxima observed at some profiles. This shift had already been observed by Booge et al. (2018) with profiles

collected during the SPACES/OASIS cruise, but not with profiles collected during the ASTRA-OMZ cruise. Booge et al. (2018) rather related this shift to enhanced mixing of isoprene, leading to a release to the water column above the MLD after production by phytoplankton. It is worth mentioning that isoprene production is probably more directly influenced by NPP than by Chla, especially if we consider the close metabolic link between isoprene production and photosynthesis. Thereby, varying Chla/C ratio with depth, often resulting in increased ratios with lower light levels at depth, would also contribute to a shift between Chla and isoprene maxima.

4.4. Importance of a Variable Consumption Rate

The relevance of using a variable bacterial consumption rate is here evaluated. For this purpose, we compare the STD-Chla experiment in which the bacterial consumption rate is constant, with the STD experiment in which it varies with Chla levels. Figures 5g and 5h show the differences between observed and simulated surface concentrations as a function of simulated Chla in the surface layer of the ocean. A clear relation between the simulated isoprene concentrations and Chla is observed with STD-Chla (expected from the Chla-dependent production term), whereas this is not the case with the observed concentrations. Hence, STD-Chla results in a degradation of the representation of surface concentrations: RMSE value is 19.2 pmol L^{-1}, against 14.5 pmol L^{-1} with STD. Indeed, regions where Chla is high (>1.0 mg m^{-3}) are overestimated by more than a factor of two. This is the case for example for the data measured during ASTRA-OMZ in October 2015 along the Peruvian coast (Booge et al., 2016). In contrast, data points located in areas where Chla is low (<0.2 mg m^{-3}) are underestimated. Below the surface, removing the Chla dependence of the consumption term results in globally higher concentrations (up to 40 pmol L^{-1}) and especially at depth where the maximum of isoprene is simulated (Figure 4, dotted green line).

The analysis of the observations did not show covariations of surface isoprene with Chla, despite what is commonly expected from a phytoplankton source. This points out that other mechanisms related to Chla might drive the ocean distribution of isoprene. A variable consumption rate may be one plausible mechanism. Using AMT vertical observed profiles, we found a significant linear correlation between the consumption rate and Chla ($R^2 = 0.54$). We assumed that the variable part of the regression corresponds to bacterial consumption of isoprene, as bacterial activity generally covaries with primary production and hence at first order also with Chla. Nevertheless, the relationship between bacterial and primary productions is not linear (Hoppe et al., 2002), and it is not known to what extent this relationship can be extended to the global ocean. The marine isoprene consumption by bacteria is indeed still poorly known, and even more its kinetic. Palmer and Shaw (2005) initially proposed to use a rate of 0.06 d^{-1} based on estimates for methyl bromide (CH_3Br) (Tokarczyk et al., 2003; Yvon-Lewis et al., 2002). However, Booge et al. (2016) obtained a better agreement between measured and modeled isoprene concentrations using a smaller rate, and their seawater incubation experiments carried out in temperature-controlled water baths showed significantly longer lifetimes (minimum of 100 days) (Booge et al., 2016) that correspond to a maximum rate of 0.01 d^{-1}. For comparison, bacterial rates retrieved from our regression analysis vary between 0 and 0.05 d^{-1} for a range of Chla of 0 to 1.0 mg m^{-3}.

The marine chemical sink of isoprene was not assumed to vary with Chla, as it is due to the reaction of isoprene in aqueous phase with major ROS: superoxide (O_2^-), hydrogen peroxide (H_2O_2), the hydroxyl radical (OH), and singlet oxygen (^{1}O2) (Palmer & Shaw, 2005). We assumed a constant rate, due to the lack of knowledge regarding both the kinetics of the reactions with isoprene in the aqueous phase and the oceanic dynamics of the ROS species. For the oxidation by OH, whereas Palmer and Shaw (2005) proposed to use a kinetic rate of 6×10^{10} (mol L^{-1})$^{-1}$ s^{-1}, Huang et al. (2011) estimated a rate that is five times slower, 1.2×10^{10} (mol L^{-1})$^{-1}$ s^{-1}, based on a specific laboratory and box model study on isoprene chemistry in water. Considering a range of oceanic OH concentrations of 10^{-18}–10^{-16} mol L^{-1} (Zinser, 2018), associated lifetimes range between 1.9 days and 2.6 years. Lifetimes associated to the oxidation by $^1O_2$ are very high: in the range 3–300 years using oceanic concentrations of 10^{-14} mol L^{-1} and a kinetic constant in the range 10^4–10^6 (mol L^{-1})$^{-1}$ s^{-1} (Riemer et al., 2000, values proposed more generally for alkenes). Lifetimes could even be longer than 316 years if one considers the concentrations reviewed in Zinser (2018) (<10^{-15} mol L^{-1}). The distributions of O_2^- and H_2O_2 are better known, and their concentrations are several orders of magnitude higher than those of OH and $^1O_2$: in the ranges 10^{-12}–10^{-10} mol L^{-1} for O_2^- and 10^{-9}–10^{-7} mol L^{-1} for

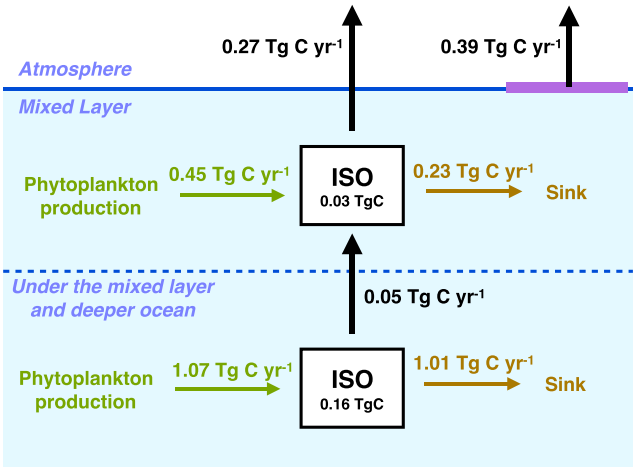

Figure 6. Global fluxes of the simulated oceanic isoprene sources and sinks, above and under the mixed layer.

H_2O_2) (Zinser, 2018 and references therein). However, there is to date no information about their reaction kinetics with isoprene in aqueous phase.

It is worth mentioning that the lack of a clear covariation between Chla and observed surface isoprene (Figures 5g and 5h) could also be explained by the production term. Indeed, as discussed above, isoprene production could be more related to NPP than to Chla. Overall, the link between isoprene and Chla needs to be better characterized, both in the production and the consumption terms. There are to date too few studies focusing on the sinks, although we show that they are as important as the sources to determine the isoprene concentrations and hence the emissions to the atmosphere.

5. Simulated Isoprene Oceanic Cycle and Fluxes to the Atmosphere

It is the first time that isoprene concentrations, and emissions to the atmosphere, are prognostically estimated using a 3D biogeochemical model. In this section, we detail the global oceanic budget of isoprene, as simulated in the STD experiment. Maps of isoprene surface concentrations and emissions to the atmosphere as well as values of the global emissions from the sensitivity experiments are available in the Supporting Information (Figure S1 and Table S1).

5.1. Global Budget and Emissions

At the scale of the global ocean, the isoprene inventory is 0.19 Tg C, with a residence time of 45.6 days. Isoprene production by phytoplankton is 1.52 Tg C yr^{-1}, of the same order of magnitude as the combined chemical and biological sinks: 1.25 Tg C yr^{-1}. The total emission of isoprene to the atmosphere is estimated to 0.66 Tg C yr^{-1} with an uncertainty range of 0.43–0.82 Tg C yr^{-1}. This value corresponds to the sum of

- the outgassing of isoprene from the ocean ($Flux_{ocean}$), 0.27 Tg C yr^{-1}, with an uncertainty range of 0.14–0.33 Tg C yr^{-1}, inferred from the sensitivity tests we performed on the processes controlling the oceanic concentrations and
- the direct emission due to photoproduction in the SML ($Flux_{SML}$), 0.39 Tg C yr^{-1}, with an uncertainty range of 0.29–0.49 Tg C yr^{-1}, based on sensitivity tests performed on the range of photochemical isoprene fluxes from marine SML and biofilm measured in laboratory studies.

Figure 6 summarizes the values of the different terms of the isoprene budget above and below the oceanic mixed layer depth. About 70.4% of the global phytoplankton production takes place below the mixed layer, and isoprene produced in these deeper layers is mainly lost there by biochemical processes. Indeed, the mean upward flux to the mixed layer is estimated to be 0.05 Tg C yr^{-1}, against 1.01 Tg C yr^{-1} estimated for the deep biochemical sink. Finally, only 15.8% of the global isoprene inventory is located above the mixed layer and can potentially escape to the atmosphere. Isoprene transported from the subsurface ocean to the mixed layer represents 18.5% of the oceanic isoprene emitted to the atmosphere (via $Flux_{ocean}$). Hence, models that assume steady state in the mixed layer (i.e., that do not represent the deeper ocean) could underestimate the emission of oceanic isoprene ($Flux_{ocean}$). This underestimation of 18.5% represents an upper limit since the change in biochemical consumption which would occur as a consequence of lower vertical input of isoprene in the mixed layer is neglected.

5.2. Spatial Dynamics

5.2.1. Integrated Sources and Sinks of Isoprene

Figure 7 displays annual mean spatial distributions of the oceanic isoprene and of the source and sink terms, all vertically integrated over the top 1,000 m of the water column. Isoprene vertical inventories are higher between 30°N and 30°S (with a mean of 8.9 μmol m^{-2}) and decrease rapidly above 60°N and °S (where the mean concentration is only 1.3 μmol m^{-2}). They are also higher in the western part of the oceanic basins, exceeding 14 μmol m^{-2} for example in the Atlantic Ocean. The isoprene spatial distribution is close to one of its source and sink terms. As a consequence of its direct dependence to Chla, integrated phytoplankton production is stronger at midlatitudes (around 100 μmol m^{-2} yr^{-1}) and weaker in the oligotrophic gyres

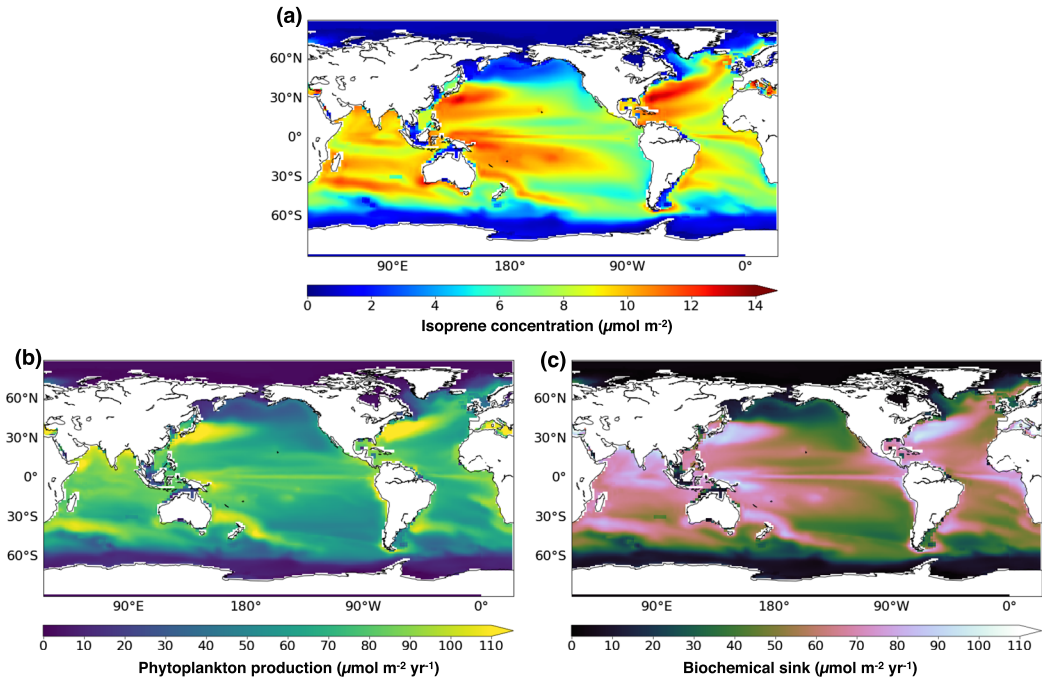

Figure 7. Spatial distribution of the oceanic isoprene (a), phytoplankton production (b), and biochemical sink (c), vertically integrated upon 1,000 m.

(around 50 μmol m^{-2} yr^{-1}). At high latitudes, production strongly decreases with latitude, falling to very low values (less than 20 μmol m^{-2} yr^{-1}) due to the additional temperature dependence. Moreover, strong production areas (exceeding 150 μmol m^{-2} yr^{-1}) are simulated in the western part of the Atlantic and Pacific basins where warm waters penetrate deeper. The isoprene sink (combined bacterial and chemical consumption) is highly dependent on the isoprene inventory with collocated integrated maxima (exceeding 110 μmol m^{-2} yr^{-1}), although the bacterial sink is relatively more intense in biologically active areas due to the Chla dependence of the bacterial consumption rate.

5.2.2. Isoprene Concentrations in the Surface Ocean and Emissions to the Atmosphere

Figures 8a and 8b present the annual mean isoprene concentrations at the surface (taken as the first 10 m) and their seasonal variations with latitude. Isoprene concentration pattern in this surface layer is slightly different from the vertically integrated one. It depends more strongly on Chla than the integrated pattern which shows a stronger temperature dependence. Indeed, surface concentrations are higher at low and midlatitudes, but strong maxima (more than 70 pmol L^{-1}) are found in the eastern equatorial Atlantic and Pacific Oceans where surface waters are enriched in nutrients by the equatorial upwelling. Also, concentrations are strongly reduced (below 10 pmol L^{-1}) in the center of the subtropical gyres. Surface isoprene concentrations present a clear seasonal cycle at midlatitudes, with maxima reached during spring in both hemispheres. At low latitudes, isoprene concentrations are rather constant throughout the year with the strongest values reached along the equator.

Figures 8c to 8h present the annual mean isoprene emissions to the atmosphere ($Flux_{ocean}$, $Flux_{SML}$ and $Flux_{tot}$) and their seasonal variations with latitude. The spatial pattern and seasonality of $Flux_{ocean}$ look similar to those of the surface isoprene concentrations. On an annual mean basis, oceanic isoprene emissions $Flux_{ocean}$ vary spatially from 0 to 117.7 nmol m^{-2} d^{-1} with a global mean flux of 28.7 nmol m^{-2} d^{-1}. With a global annual mean flux of 41.4 nmol m^{-2} d^{-1}, isoprene emissions from the SML ($Flux_{SML}$) are only slightly stronger. However, spatial patterns differ, with stronger emissions at low latitudes and stronger seasonality at midlatitudes, due to its dependence on the incident UV radiation. Finally, total isoprene emissions to the atmosphere ($Flux_{tot}$) vary spatially from 0.4 to 214.1 nmol m^{-2} d^{-1} (with a mean value of 70.1 nmol m^{-2} d^{-1}). The strongest emissions are simulated in the equatorial region (the 15°N–15°S band contributes to more than 36% to the global annual emission) and at latitudes between 30° and 60°

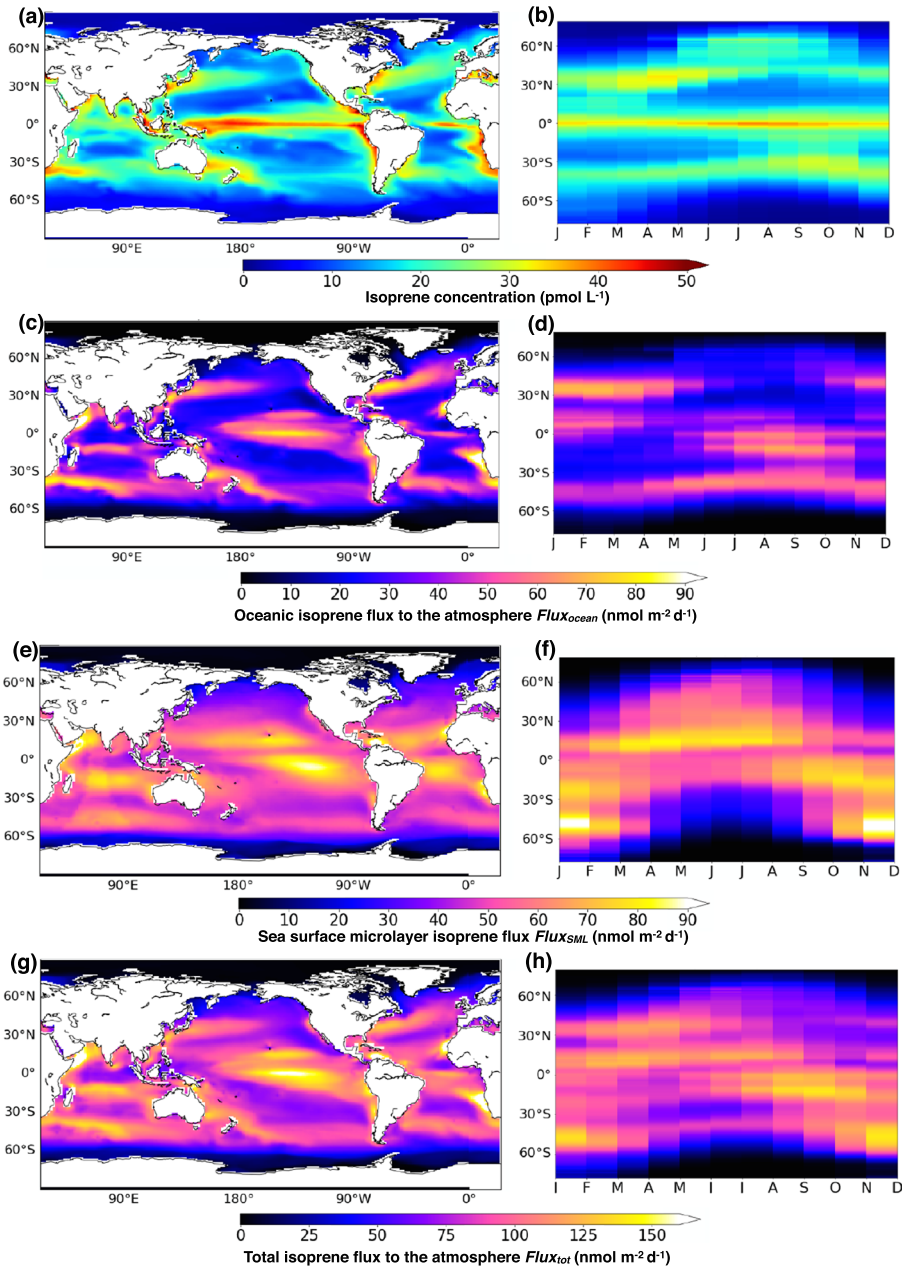

Figure 8. Oceanic isoprene concentration between 0 and 10 m (a and b), oceanic isoprene flux to the atmosphere $Flux_{ocean}$ (c and d), sea surface microlayer flux $Flux_{SML}$ (e and f), and total flux to the atmosphere $Flux_{tot}$ (g and h). (a, c, e, and g) Spatial distribution of the annual mean. (b, d, f, and h) Mean seasonal variation with latitude.

(contributing to more than 38% to the global annual emissions). High emissions are also reached locally along the west coast of South America and Africa. Annual mean emissions are strongly reduced above 60° north or south (those combined two regions contribute to only 2% to the global annual emission).

5.2.3. Flux From the Subsurface

Globally, most of the isoprene production takes place under the mixed layer, but only 0.05 Tg C yr^{-1} of this isoprene is transported upwards to the mixed layer. In order to investigate the spatial variability of this vertical upward flux, we calculated for every modeled water column the integrals of isoprene sources and sinks above and below the mixed layer depth, from which we deduced the local mean subsurface flux assuming both equilibrium and no horizontal transport of isoprene. Figure 9 presents spatially the importance of

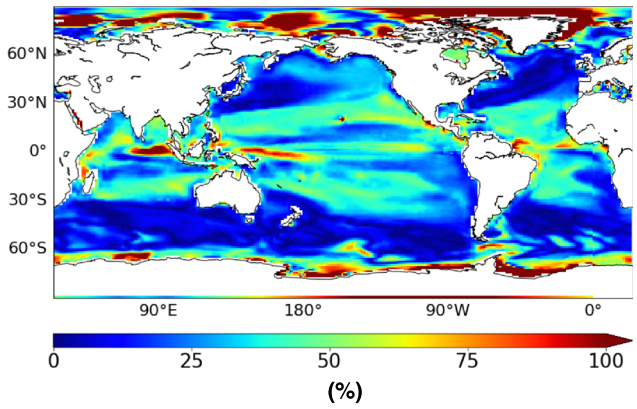

Figure 9. Spatial distribution of the mean annual ratio between the estimated isoprene subsurface flux and the simulated oceanic isoprene flux to the atmosphere $Flux_{ocean}$ (as a percentage).

this subsurface flux, expressed as a percentage of the oceanic isoprene flux to the atmosphere ($Flux_{ocean}$). In the equatorial region, the subsurface flux of isoprene to the mixed layer can exceed 50% of $Flux_{ocean}$. This is due to enhanced mixing around the equatorial divergence, bringing up more isoprene to the surface layer. In the center of the Pacific and Atlantic oligotrophic gyres, although emissions are highly reduced, percentage can also exceed 50% due to isoprene production occurring mostly below the mixed layer. In those regions, there is hence an importance of representing the subsurface production for estimating the ocean-atmosphere exchanges in this region. In contrast, around 30° and 60° north or south, outgassing of isoprene is high, but there is a limited contribution of the subsurface production (percentage is less than 25%).

5.3. Comparison to Previous Studies

The global oceanic isoprene emission ($Flux_{ocean}$, i.e., before applying isoprene emissions from the SML) is estimated with PISCES to 0.27 (0.14–0.33) Tg C yr^{-1}. This value is in the range of previous bottom-up estimates, 0.1–1.2 Tg C yr^{-1}, which do not account for the SML isoprene emission (Arnold et al., 2009; Bonsang et al., 1992; Booge et al., 2016; Gantt et al., 2009; Palmer & Shaw, 2005; Sinha et al., 2007) (Table 1). Our simulated emission $Flux_{ocean}$ can be compared with other spatialized emissions from Palmer and Shaw (2005), Gantt et al. (2009), and Booge et al. (2016). Overall, as all other formerly published isoprene distributions, our simulated spatiotemporal dynamic is first driven by Chla (with higher emissions around the equator, in coastal upwelling systems, and at midlatitudes). This is not surprising provided that all parameterizations are based on the assumption that isoprene production is proportional to Chla. A strict matching between Chla and emissions is found by Palmer and Shaw (2005), who applied a single constant production rate with Chla, with a sink proportional to the simulated isoprene concentration. However, the relative magnitude of the emissions in the different regions varies from one estimation to another. In our model, oceanic emissions are strong around the equator, as a consequence of the temperature and Chla dependencies and, to a lesser extent, due to the fact that diatom production rates are lower than those of nanophytoplankton. Booge et al. (2016) produced a global estimate of the emission of 0.21 Tg C yr^{-1} with a PFT-dependent relationship. Their emissions are largely increased at high latitudes (around both 60°N and 60°S), due to a strong production rate assigned to diatoms. This leads to annual mean emissions exceeding 90 nmol m^2 d^{-1} in the north Atlantic, whereas in PISCES, oceanic emissions in this region are lower than 20 nmol m^2 d^{-1}. Around the equator, their emissions are strongly reduced (less than 30 nmol m^2 d^{-1}), whereas in PISCES, they can reach 80 nmol m^2 d^{-1}. Gantt et al. (2009) implemented relationships which, in addition to PFTs, also depend on incident PAR and produced a global estimate of 0.92 Tg C yr^{-1}. This estimate is higher than what is predicted by PISCES. However, Gantt et al. (2009) calculated an uncertainty range due to PFT speciation of 0.31–1.09 Tg C yr^{-1}. Their patterns present strengthened emissions at low latitudes (and tropics due to high irradiance despite the relatively low Chla levels), with a stronger seasonality at midlatitudes due to both high irradiance and Chla.

The global SML isoprene emission ($Flux_{SML}$) is estimated to 0.39 (0.29–0.49) Tg C yr^{-1}, with an uncertainty. Spatial pattern of this flux resembles the pattern of the photochemical emission potential produced by Brüggemann et al. (2018). However, their global estimate of the isoprene SML emission is higher: 0.98 (0.62–1.34) Tg C yr^{-1}. This difference could be due to an underestimation of the NPP. Indeed, the annual NPP predicted with PISCES is 44 Gt C yr^{-1}, which falls on the lower bound of the estimates retrieved from satellite observations: 37 and 67 Gt C yr^{-1} (Aumont et al., 2015 and references therein). The total isoprene emission to the atmosphere ($Flux_{tot}$) is estimated to 0.66 (0.43–0.82) Tg C yr^{-1}, which is still below the range of top-down estimates: 1.5–11.6 Tg C yr^{-1} (Arnold et al., 2009; Hu et al., 2013; Luo & Yu, 2010). Hence, the addition of an isoprene flux due to interfacial photochemistry only helped in minimizing this discrepancy. Both uncertainties in the top-down estimates and on the interfacial photochemistry may play a role in the difficulties to reconcile the two approaches. In particular, whereas the SML plays a central role in a range of physical, biogeochemical, and climate-related processes (Cunliffe et al., 2013), high uncertainties on its spatiotemporal dynamic, on the complex nature of its surfactants, and on the impact of these surfactants

Table 1
Bottom-up Estimates of the Global Annual Flux of Isoprene to the Atmosphere, Described in the Literature and in this Study

	Global oceanic isoprene flux to the atmosphere in Tg C yr^{-1} (range)	Global sea surface microlayer isoprene flux in Tg C yr^{-1} (range)	Type of study	Origin of the Chla field and temporal coverage	Production term	Biochemical sink term
This study	0.27 (0.14–0.33)	0.39 (0.29–0.49)	3D modeling	Chla is computed prognostically Mean climatology	Variable rates with PFTs (two groups) and temperature	Variable rate with Chla
Booge et al. (2016)	0.21	Not represented	2D modeling	Monthly mean satellite data (MODIS) for 2014	Variable rates with PFTs (four groups)	Constant rate
Luo and Yu (2010)	0.32			Monthly mean satellite data (merged of MODIS and SeaWiFS products) for 2006	Variable rates with PFTs (four groups)	No sink
Gantt et al. (2009)	0.92 (0.31–1.09)			Monthly mean satellite data (SeaWiFS) for 2001	Variable rates with PFTs (four groups) and incoming PAR radiation	No sink
Arnold et al. (2009)	0.27 (± 0.07)			Monthly mean satellite data (SeaWiFS) for 2000	Variable rates with PFTs (four groups)	No sink
Palmer and Shaw (2005)	0.1			Monthly mean satellite data (MODIS) for 2001	Constant rate	Constant rate
Sinha et al. (2007)	1.2	Not represented	Global extrapolation of in situ isoprene measurements (May/June 2005)			
Bonsang et al. (1992)	1.1		Global extrapolation of in situ isoprene measurements (May/June 1987, October 1989, and April/May 1990)			

on air-sea gas exchanges lead to highly underconstrained SML fluxes parameterizations. Uncertainties in the oceanic isoprene emission ($Flux_{ocean}$) may also be important. However, as those latter reflect the simulated isoprene concentrations, which were fitted according to observed concentrations, this source of uncertainty may not be the only reason for this discrepancy.

6. Conclusion and Perspectives

In this study, we first explored different parameterizations of the oceanic isoprene sources and sinks, based on experimental, field, and theoretical knowledge. We show that seawater temperature is the most important driver of isoprene phytoplankton production for best representing the in situ surface and vertical isoprene concentrations. Regarding the importance of irradiance, results are very ambiguous. Whereas this parameter could partly explain the observed shift between isoprene and Chla maxima at depth, it leads to very low concentrations at depth and does not contribute to better represent the surface data. Finally, the exploration of a variable consumption term shows a potential link between the biochemical sink and phytoplankton activity. Second, we provide the first global estimates of the oceanic isoprene cycle based on a 3D model. We show that most of the isoprene production occurs below the mixed layer. As a consequence, other bottom-up models based on 2D surface Chla could miss up to 18.5% of the global emission of oceanic isoprene and even more in some specific locations such as the equatorial Pacific. Our estimate of the isoprene flux to the atmosphere due to the production occurring in the water column is 0.27 (0.14–0.33) Tg C yr^{-1}. It is in the range of previous bottom-up estimates based on satellite-retrieved maps of monthly means Chla or on global extrapolation of in situ measurements. We also represent for the first time in an oceanic isoprene model the flux due to photochemical processes occurring in the SML (in addition to the oceanic flux). This SML flux is estimated to 0.39 (0.29–0.49) Tg C yr^{-1}, producing a total isoprene flux to the atmosphere of 0.66 (0.43–0.82) Tg C yr^{-1}.

A lot of uncertainties remain on our knowledge of processes, both quantitatively and qualitatively, which strongly limits our current capability to model the marine cycle of isoprene and to produce accurate estimates of the global fluxes to the atmosphere. In particular, there is a large variability in Chla-normalized production rates retrieved from laboratory experiments. More experiments are needed not only to increase the number of estimates per PFT, but also to derive specific relations with environmental drivers. There is

also a strong lack of studies focusing on the oceanic biochemical sink of isoprene, although it is as important as production to accurately estimate ocean isoprene. Better constraining the terms controlling the 3D oceanic isoprene is necessary to reduce the discrepancies between observed and simulated concentrations. However, since the parameterizations we used are tuned to fit the in situ observations, it seems that for bridging the gap between top-down and bottom-up estimates of the emission to the atmosphere, priority should be put on both refining the top-down estimates and on better constraining the SML photoproduction of isoprene.

Acknowledgments

We would like to thank the LEFE FORCAGE and EU-H2020-CRESCENDO (grant agreement 641816) projects for funding. We also gratefully acknowledge Dennis Booge for providing us isoprene surface data from the ASTRA-OMZ, SPACES/OASIS, and ANT-XXV/1 cruises; Sina Hackenberg, Lucy Carpenter, Ally Lewis, and the British Oceanographic Data center for providing us data from the AMT22, AMT23, and ACCACIA cruises (https://www.bodc.ac.uk/data/bodc_database/nodb/); and Bernard Bonsang and Cédric Fichot for their contribution. A first version of the work was performed during the internship of Aïda Bellataf in 2012 with the help of Sophie Tran. The authors are thankful to them and have a thought to Aïda, a very dynamic and enthusiastic student who brutally died in 2017 at the age of 32. Finally, we thank the ASTM for the distribution of the ground-based solar spectral irradiance SMARTS2 (version 2.9.2) *Simple Model for Atmospheric Transmission of Sunshine* (https://www.astm.org/Standards/G173.htm). TRANSSIZ data were obtained during the ARKXXIX/1-PS92 TRANSSIZ cruise (*Transitions in the Arctic Seasonal Sea Ice Zone*), under the grant AWI_PS92_00. This work was granted access to the HPC resources of TGCC under the allocation 2017-A0050102201 and 2017-A0050100040 made by GENCI (Grand Equipement National de Calcul Intensif).

References

Alvain, S., Moulin, C., Dandonneau, Y., & Bréon, F. M. (2005). Remote sensing of phytoplankton groups in case 1 waters from global SeaWiFS imagery. *Deep Sea Research Part I: Oceanographic Research Papers*, *52*(11), 1989–2004. https://doi.org/10.1016/j.dsr.2005.06.015

Alvarez, L. A., Exton, D. A., Timmis, K. N., Suggett, D. J., & McGenity, T. J. (2009). Characterization of marine isoprene-degrading communities. *Environmental Microbiology*, *11*(12), 3280–3291. https://doi.org/10.1111/j.1462-2920.2009.02069.x

Anttila, T., Langmann, B., Varghese, S., & O'Dowd, C. (2010). Contribution of isoprene oxidation products to marine aerosol over the North-East Atlantic. *Advances in Meteorology*, *2010*, 1–10. https://doi.org/10.1155/2010/482603

Arneth, A., Monson, R. K., Schurgers, G., Niinemets, Ü., & Palmer, P. I. (2008). Why are estimates of global terrestrial isoprene emissions so similar (and why is this not so for monoterpenes)? *Atmospheric Chemistry and Physics*, *8*(16), 4605–4620. https://doi.org/10.5194/acp-8-4605-2008

Arneth, A., Niinemets, Ü., Pressley, S., Bäck, J., Hari, P., Karl, T., et al. (2007). Process-based estimates of terrestrial ecosystem isoprene emissions: Incorporating the effects of a direct CO2-isoprene interaction. *Atmospheric Chemistry and Physics*, *7*, 31–53. https://doi.org/10.5194/acp-7-31-2007

Arnold, S. R., Spracklen, D. V., Williams, J., Yassaa, N., Sciare, J., Bonsang, B., et al. (2009). Evaluation of the global oceanic isoprene source and its impacts on marine organic carbon aerosol. *Atmospheric Chemistry and Physics*, *9*, 1253–1262. https://doi.org/10.5194/acp-9-1253-2009

ASTM (2012). *G173-03 (2012), Standard Tables for Reference Solar Spectral Irradiances: Direct Normal and Hemispherical on 37° Tilted Surface*. West Conshohocken, PA: ASTM International. www.astm.org

Atkinson, R. (2000). Atmospheric chemistry of VOCs and NOx. *Atmospheric Environment*, *34*(12-14), 2063–2101. https://doi.org/10.1016/S1352-2310(99)00460-4

Aumont, O., Ethé, C., Tagliabue, A., Bopp, L., & Gehlen, M. (2015). PISCES-v2: An ocean biogeochemical model for carbon and ecosystem studies. *Geoscientific Model Development*, *8*(8), 2465–2513. https://doi.org/10.5194/gmd-8-2465-2015

Baker, A. R., Turner, S. M., Broadgate, W. J., Thompson, A., McFiggans, G. B., Vesperini, O., et al. (2000). Distribution and sea-air fluxes of biogenic trace gases in the eastern Atlantic Ocean. *Global Biogeochemical Cycles*, *14*, 871–886. https://doi.org/10.1029/1999GB001219

Ben Mustapha, Z., Alvain, S., Jamet, C., Loisel, H., & Dessailly, D. (2014). Automatic classification of water-leaving radiance anomalies from global SeaWiFS imagery: Application to the detection of phytoplankton groups in open ocean waters. *Remote Sensing of Environment*, *146*, 97–112. https://doi.org/10.1016/j.rse.2013.08.046

Bonsang, B., Gros, V., Peeken, I., Yassaa, N., Bluhm, K., Zoellner, E., et al. (2010). Isoprene emission from phytoplankton monocultures: The relationship with chlorophyll-*a*, cell volume and carbon content. *Environmental Chemistry*, *7*(6), 554. https://doi.org/10.1071/EN09156

Bonsang, B., Polle, C., & Lambert, G. (1992). Evidence for marine production of isoprene. *Geophysical Research Letters*, *19*(11), 1129–1132. https://doi.org/10.1029/92GL00083

Booge, D., Marandino, C. A., Schlundt, C., Palmer, P. I., Schlundt, M., Atlas, E. L., et al. (2016). Can simple models predict large-scale surface ocean isoprene concentrations? *Atmospheric Chemistry and Physics*, *16*(18), 11,807–11,821. https://doi.org/10.5194/acp-16-11807-2016

Booge, D., Schlundt, C., Bracher, A., Endres, S., Zäncker, B., & Marandino, C. A. (2018). Marine isoprene production and consumption in the mixed layer of the surface ocean—A field study over two oceanic regions. *Biogeosciences*, *15*(2), 649–667. https://doi.org/10.5194/bg-15-649-2018

Broadgate, W. J., Liss, P. S., & Penkett, S. A. (1997). Seasonal emissions of isoprene and other reactive hydrocarbon gases from the ocean. *Geophysical Research Letters*, *24*(21), 2675–2678. https://doi.org/10.1029/97GL02736

Brüggemann, M., Hayeck, N., Bonnineau, C., Pesce, S., Alpert, P. A., Perrier, S., et al. (2017). Interfacial photochemistry of biogenic surfactants: A major source of abiotic volatile organic compounds. *Faraday Discussions*, *200*, 59–74. https://doi.org/10.1039/C7FD00022G

Brüggemann, M., Hayeck, N., & George, C. (2018). Interfacial photochemistry at the ocean surface is a global source of organic vapors and aerosols. *Nature Communications*, *9*(1), 2101. https://doi.org/10.1038/s41467-018-04528-7

Carslaw, K. S., Boucher, O., Spracklen, D. V., Mann, G. W., Rae, J. G. L., Woodward, S., & Kulmala, M. (2010). A review of natural aerosol interactions and feedbacks within the Earth system. *Atmospheric Chemistry and Physics*, *10*(4), 1701–1737. https://doi.org/10.5194/acp-10-1701-2010

Ciuraru, R., Fine, L., van Pinxteren, M., D'Anna, B., Herrmann, H., & George, C. (2015a). Photosensitized production of functionalized and unsaturated organic compounds at the air-sea interface. *Scientific Reports*, *5*(1), 12741. https://doi.org/10.1038/srep12741

Ciuraru, R., Fine, L., van Pinxteren, M., D'Anna, B., Herrmann, H., & George, C. (2015b). Unravelling new processes at interfaces: Photochemical isoprene production at the sea surface. *Environmental Science & Technology*, *49*(22), 13,199–13,205. https://doi.org/10.1021/acs.est.5b02388

Claeys, M. (2004). Formation of secondary organic aerosols through photooxidation of isoprene. *Science*, *303*(5661), 1173–1176. https://doi.org/10.1126/science.1092805

Cleveland, C. C., & Yavitt, J. B. (1997). Consumption of atmospheric isoprene in soil. *Geophysical Research Letters*, *24*(19), 2379–2382. https://doi.org/10.1029/97GL02451

Cleveland, C. C., & Yavitt, J. B. (1998). Microbial consumption of atmospheric isoprene in a temperate forest soil. *Applied and Environmental Microbiology*, *64*(1), 172–177. https://aem.asm.org/content/64/1/172.short, https://doi.org/10.1128/AEM.64.1.172-177.1998

Colomb, A., Yassaa, N., Williams, J., Peeken, I., & Lochte, K. (2008). Screening volatile organic compounds (VOCs) emissions from five marine phytoplankton species by head space gas chromatography/mass spectrometry (HS-GC/MS). *Journal of Environmental Monitoring*, *10*(3), 325–330. https://doi.org/10.1039/b715312k

Conkright, M. E., Locarnini, R. A., Garcia, H. E., O'Brien, T. D., Boyer, T. P., Stephens, C., & Antononov, J. (2002). World Ocean Atlas 2001: Objective analyses, data statistics and figures, CD-ROM documentation, Tech. rep., National Oceanographic Data Centre, Silver Spring, MD, USA, 2002, https://repository.library.noaa.gov/view/noaa/1174

Cunliffe, M., Engel, A., Frka, S., Gašparovi, B., Guitart, C., Murrell, J. C., et al. (2013). Sea surface microlayers: A unified physicochemical and biological perspective of the air-ocean interface. *Progress in Oceanography*, *109*, 104–116. https://doi.org/10.1016/j.pocean.2012.08.004

Dani, K. G. S., & Loreto, F. (2017). Trade-off between dimethyl sulfide and isoprene emissions from marine phytoplankton. *Trends in Plant Science*, *22*(5), 361–372. https://doi.org/10.1016/j.tplants.2017.01.006

El Khawand, M., Crombie, A. T., Johnston, A., Vavlline, D. V., McAuliffe, J. C., Latone, A., & Murrell, J. C. (2016). Isolation of isoprene degrading bacteria from soils, development of isoA gene probes and identification of the active isoprene-degrading soil community using DNA-stable isotope probing. *Environmental Microbiology*, *18*(8), 2743–2753. https://doi.org/10.1111/1462-2920.13345

Ewers, J., Freier-Schröder, D., & Knackmuss, H. J. (1990). Selection of trichloroethene (TCE) degrading bacteria that resist inactivation by TCE. *Archives of Microbiology*, *154*(4), 410–413. https://doi.org/10.1007/BF00276540

Exton, D. A., Suggett, D. J., McGenity, T. J., & Steinke, M. (2013). Chlorophyll-normalized isoprene production in laboratory cultures of marine microalgae and implications for global models. *Limnology and Oceanography*, *58*(4), 1301–1311. https://doi.org/10.4319/lo.2013.58.4.1301

Ferrieri, R. A., Gray, D. W., Babst, B. A., Schueller, M. J., Schlyer, D. J., Thorpe, M. R., et al. (2005). Use of carbon-11 in Populus shows that exogenous jasmonic acid increases biosynthesis of isoprene from recently fixed carbon. *Plant, Cell & Environment*, *28*(5), 591–602. https://doi.org/10.1111/j.1365-3040.2004.01303.x

Flombaum, P., Gallegos, J. L., Gordillo, R. A., Rincon, J., Zabala, L. L., Jiao, N., et al. (2013). Present and future global distributions of the marine cyanobacteria Prochlorococcus and Synechococcus. *Proceedings of the National Academy of Sciences*, *110*(24), 9824–9829. https://doi.org/10.1073/pnas.1307701110

Gantt, B., Meskhidze, N., & Kamykowski, D. (2009). A new physically-based quantification of marine isoprene and primary organic aerosol emissions. *Atmospheric Chemistry and Physics*, *9*(14), 4915–4927. https://doi.org/10.5194/acp-9-4915-2009

Geider, R. J., MacIntyre, H. L., & Kana, T. M. (1996). A dynamic model of photoadaptation in phytoplankton. *Limnology and Oceanography*, *41*(1), 1–15. https://doi.org/10.4319/lo.1996.41.1.0001

Gray, C. M., Helmig, D., & Fierer, N. (2015). Bacteria and fungi associated with isoprene consumption in soil. *Elem Sci Anth*, *3*, 000053. https://doi.org/10.12953/journal.elementa.000053

Gros, V., & Bonsang, B. (2019). Isoprene concentrations in the surface South Atlantic waters during Marion Dufresne cruise MD160 (OOMPH MD07 leg 2) in March 2007, PANGAEA. https://doi.org/10.1594/PANGAEA.905172

Gros, V., Sarda-Estève, R., & Bonsang, B. (2019). Isoprene concentrations in the surface Arctic waters during POLARSTERN cruise PS92 (ARK-XXIX/1 TRANSSIZ) in May 2015, PANGAEA. https://doi.org/10.1594/PANGAEA.905170

Guenther, A., Karl, T., Harley, P., Wiedinmyer, C., Palmer, P. I., & Geron, C. (2006). Estimates of global terrestrial isoprene emissions using MEGAN (model of emissions of gases and aerosols from nature). *Atmospheric Chemistry and Physics*, *6*(11), 3181–3210. https://doi.org/10.5194/acp-6-3181-2006

Guenther, A. B., Monson, R. K., & Fall, R. (1991). Isoprene and monoterpene emission rate variability: Observations with eucalyptus and emission rate algorithm development. *Journal of Geophysical Research*, *96*(D6), 10,799–10,808. https://doi.org/10.1029/91JD00960

Hackenberg, S. C., Andrews, S. J., Airs, R., Arnold, S. R., Bouman, H. A., Brewin, R. J. W., et al. (2017). Potential controls of isoprene in the surface ocean. *Isoprene Controls in the Surface Ocean, Global Biogeochemical Cycles*, *31*(4), 644–662. https://doi.org/10.1002/2016GB005531

Hoppe, H. G., Gocke, K., Koppe, R., & Begler, C. (2002). Bacterial growth and primary production along a north–south transect of the Atlantic Ocean. *Nature*, *416*(6877), 168–171. https://doi.org/10.1038/416168a

Hu, Q.-H., Xie, Z.-Q., Wang, X.-M., Kang, H., He, Q.-F., & Zhang, P. (2013). Secondary organic aerosols over oceans via oxidation of isoprene and monoterpenes from Arctic to Antarctic. *Scientific Reports*, *3*(1), 2280. https://doi.org/10.1038/srep02280

Huang, D., Zhang, X., Chen, Z. M., Zhao, Y., & Shen, X. L. (2011). The kinetics and mechanism of an aqueous phase isoprene reaction with hydroxyl radical. *Atmospheric Chemistry and Physics*, *11*(15), 7399–7415. https://doi.org/10.5194/acp-11-7399-2011

Johnston, A., Crombie, A. T., El Khawand, M., Sims, L., Whited, G. M., McGenity, T. J., & Colin Murrell, J. (2017). Identification and characterisation of isoprene-degrading bacteria in an estuarine environment: Estuarine isoprene-degrading bacteria. *Environmental Microbiology*, *19*(9), 3526–3537. https://doi.org/10.1111/1462-2920.13842

Kameyama, S., Yoshida, S., Tanimoto, H., Inomata, S., Suzuki, K., & Yoshikawa-Inoue, H. (2014). High-resolution observations of dissolved isoprene in surface seawater in the Southern Ocean during austral summer 2010–2011. *Journal of Oceanography*, *70*(3), 225–239. https://doi.org/10.1007/s10872-014-0226-8

Kroll, J. H., Ng, N. L., Murphy, S. M., Flagan, R. C., & Seinfeld, J. H. (2006). Secondary organic aerosol formation from isoprene photooxidation. *Environmental Science & Technology*, *40*(6), 1869–1877. https://doi.org/10.1021/es0524301

Kurihara, M., Iseda, M., Ioriya, T., Horimoto, N., Kanda, J., Ishimaru, T., et al. (2012). Brominated methane compounds and isoprene in surface seawater of Sagami Bay: Concentrations, fluxes, and relationships with phytoplankton assemblages. *Marine Chemistry*, *134-135*, 71–79. https://doi.org/10.1016/j.marchem.2012.04.001

Kurihara, M. K., Kimura, M., Iwamoto, Y., Narita, Y., Ooki, A., Eum, Y. J., et al. (2010). Distributions of short-lived iodocarbons and biogenic trace gases in the open ocean and atmosphere in the western North Pacific. *Marine Chemistry*, *118*(3-4), 156–170. https://doi.org/10.1016/j.marchem.2009.12.001

Lichtenthaler, H. K. (2009). Biosynthesis and accumulation of isoprenoid carotenoids and chlorophylls and emission of isoprene by leaf chloroplasts. *Bulletin of the Georgian National Academy of Sciences*, *3*, 81–94.

Lichtenthaler, H. K., Schwender, J., Disch, A., & Rohmer, M. (1997). Biosynthesis of isoprenoids in higher plant chloroplasts proceeds via a mevalonate-independent pathway. *FEBS Letters*, *400*(3), 271–274. https://doi.org/10.1016/s0014-5793(96)01404-4

Logan, B. A., Monson, R. K., & Potosnak, M. J. (2000). Biochemistry and physiology of foliar isoprene production. *Trends in plant science*, *5*, 477–481. https://doi.org/10.1016/S1360-1385(00)01765-9

Lohr, M., Schwender, J., & Polle, J. E. W. (2012). Isoprenoid biosynthesis in eukaryotic phototrophs: A spotlight on algae. *Plant Science*, *185-186*, 9–22. https://doi.org/10.1016/j.plantsci.2011.07.018

Loreto, F., & Fineschi, S. (2015). Reconciling functions and evolution of isoprene emission in higher plants. *New Phytologist*, *206*(2), 578–582. https://doi.org/10.1111/nph.13242

Loreto, F., & Schnitzler, J.-P. (2010). Abiotic stresses and induced BVOCs. *Trends in Plant Science*, *15*(3), 154–166. https://doi.org/10.1016/j.tplants.2009.12.006

Luo, G., & Yu, F. (2010). A numerical evaluation of global oceanic emissions of α-pinene and isoprene. *Atmospheric Chemistry and Physics*, *10*(4), 2007–2015. https://doi.org/10.5194/acp-10-2007-2010

Madec, G. (2008). NEMO Ocean Engine, Note du Pôle de Modélisation, Institut Pierre-Simon Laplace (IPSL), France, http://www.nemo-ocean.eu, 2008.

Matsunaga, S., Mochida, M., Saito, T., & Kawamura, K. (2002). In situ measurement of isoprene in the marine air and surface seawater from the western North Pacific. *Atmospheric Environment*, *36*(39-40), 6051–6057. https://doi.org/10.1016/S1352-2310(02)00657-X

McGillis, W. R., Edson, J. B., Zappa, C. J., Ware, J. D., McKenna, S. P., Terray, E. A., et al. (2004). Air-sea CO_2 exchange in the equatorial Pacific. *Journal of Geophysical Research*, *109*, C08S02. https://doi.org/10.1029/2003JC002256

McKay, W. A., Turner, M. F., Jones, B. M. R., & Halliwell, C. M. (1996). Emissions of hydrocarbons from marine phytoplankton—Some results from controlled laboratory experiments. *Atmospheric Environment*, *30*(14), 2583–2593. https://doi.org/10.1016/1352-2310(95)00433-5

Meskhidze, N., & Nenes, A. (2006). Phytoplankton and cloudiness in the Southern Ocean. *Science*, *314*(5804), 1419–1423. https://doi.org/10.1126/science.1131779

Meskhidze, N., Sabolis, A., Reed, R., & Kamykowski, D. (2015). Quantifying environmental stress-induced emissions of algal isoprene and monoterpenes using laboratory measurements. *Biogeosciences*, *12*(3), 637–651. https://doi.org/10.5194/bg-12-637-2015

Milne, P. J., Riemer, D. D., Zika, R. G., & Brand, L. E. (1995). Measurement of vertical distribution of isoprene in surface seawater, its chemical fate, and its emission from several phytoplankton monocultures. *Marine Chemistry*, *48*(3-4), 237–244. https://doi.org/10.1016/0304-4203(94)00059-M

Mochalski, P., King, J., Kupferthaler, A., Unterkofler, K., Hinterhuber, H., & Amann, A. (2011). Measurement of isoprene solubility in water, human blood and plasma by multiple headspace extraction gas chromatography coupled with solid phase microextraction. *Journal of Breath Research*, *5*(4), 046010. https://doi.org/10.1088/1752-7155/5/4/046010

Moore, R. M., Oram, D. E., & Penkett, S. A. (1994). Production of isoprene by marine phytoplankton cultures. *Geophysical Research Letters*, *21*(23), 2507–2510. https://doi.org/10.1029/94GL02363

Müller, J.-F., Stavrakou, T., Wallens, S., De Smedt, I., Van Roozendael, M., Potosnak, M. J., et al. (2008). Global isoprene emissions estimated using MEGAN, ECMWF analyses and a detailed canopy environment model. *Atmospheric Chemistry and Physics*, *8*, 1329–1341. https://doi.org/10.5194/acp-8-1329-2008

Myriokefalitakis, S., Vignati, E., Tsigaridis, K., Papadimas, C., Sciare, J., & Mihalopoulos, N. (2010). Global modeling of the oceanic source of organic aerosols. *Advances in Meteorology*, 2010, 1–16. https://doi.org/10.1155/2010/939171

Ooki, A., Nomura, D., Nishino, S., Kikuchi, T., & Yokouchi, Y. (2015). A global-scale map of isoprene and volatile organic iodine in surface seawater of the Arctic. *Northwest Pacific, Indian, and Southern Oceans: a global-scale map of isoprene and VOI, Journal of Geophysical Research: Oceans*, *120*, 4108–4128. https://doi.org/10.1002/2014JC010519

Palmer, P. I., & Shaw, S. L. (2005). Quantifying global marine isoprene fluxes using MODIS chlorophyll observations. *Geophysical Research Letters*, *32*, L09805. https://doi.org/10.1029/2005GL022592

Pollastri, S., Tsonev, T., & Loreto, F. (2014). Isoprene improves photochemical efficiency and enhances heat dissipation in plants at physiological temperatures. *Journal of Experimental Botany*, *65*(6), 1565–1570. https://doi.org/10.1093/jxb/eru033

Riemer, D. D., Milne, P. J., Zika, R. G., & Pos, W. H. (2000). Photoproduction of nonmethane hydrocarbons (NMHCs) in seawater. *Marine Chemistry*, *71*(3-4), 177–198. https://doi.org/10.1016/S0304-4203(00)00048-7

Sanadze, G. A. (2004). Biogenic isoprene (a review). *Russian Journal of Plant Physiology*, *51*(6), 729–741. https://doi.org/10.1023/B:RUPP.0000047821.63354.a4

Schnitzler, J.-P. (2004). Contribution of different carbon sources to isoprene biosynthesis in poplar leaves. *Plant Physiology*, *135*(1), 152–160. https://doi.org/10.1104/pp.103.037374

Schwender, J., Seemann, M., Lichtenthaler, H. K., & Rohmer, M. (1996). Biosynthesis of isoprenoids (carotenoids, sterols, prenyl side-chains of chlorophylls and plastoquinone) via a novel pyruvate/glyceraldehyde 3-phosphate non-mevalonate pathway in the green alga *Scenedesmus obliquus*. *Biochemical Journal*, *316*(1), 73–80. https://doi.org/10.1042/bj3160073

Sharkey, T. D., & Monson, R. K. (2017). Isoprene research—60 years later, the biology is still enigmatic: Isoprene research. *Plant, Cell & Environment*, *40*(9), 1671–1678. https://doi.org/10.1111/pce.12930

Sharkey, T. D., Singsaas, E. L., Vanderveer, P. J., & Geron, C. (1995). Field measurements of isoprene emission from trees in response to temperature and light. *Tree Physiology*, *16*(7), 649–654. https://doi.org/10.1093/treephys/16.7.649

Sharkey, T. D., Wiberley, A. E., & Donohue, A. R. (2008). Isoprene emission from plants: Why and how. *Annals of Botany*, *101*(1), 5–18. https://doi.org/10.1093/aob/mcm240

Sharkey, T. D., & Yeh, S. (2001). Isoprene emission from plants. *Annual Review of Plant Biology*, *52*(1), 407–436. https://doi.org/10.1146/annurev.arplant.52.1.407

Shaw, S. L., Chisholm, S. W., & Prinn, R. G. (2003). Isoprene production by Prochlorococcus, a marine cyanobacterium, and other phytoplankton. *Marine Chemistry*, *80*, 227–245. https://doi.org/10.1016/S0304-4203(02)00101-9

Sinha, V., Williams, J., Meyerhöfer, M., Riebesell, U., Paulino, A. I., & Larsen, A. (2007). Air-sea fluxes of methanol, acetone, acetaldehyde, isoprene and DMS from a Norwegian fjord following a phytoplankton bloom in a mesocosm experiment. *Atmospheric Chemistry and Physics*, *7*(3), 739–755. http://www.atmos-chem-phys.net/7/739/2007/acp-7-739-2007.html, https://doi.org/10.5194/acp-7-739-2007

Srivastva, N., Singh, A., Bhardwaj, Y., & Dubey, S. K. (2017). Biotechnological potential for degradation of isoprene: A review. *Critical Reviews in Biotechnology*, *38*(4), 587–599. https://doi.org/10.1080/07388551.2017.1379467

Tingey, D. T., Turner, D. P., & Weber, J. A. (1991). *Factors controlling the emissions of monoterpenes and other volatile organic compounds*. Washington, D. C: U.S. Environmental Protection Agency. https://doi.org/10.1016/B978-0-12-639010-0.50009-1

Tokarczyk, R., Goodwin, K. D., & Saltzman, E. S. (2003). Methyl chloride and methyl bromide degradation in the Southern Ocean: Methyl chloride oceanic degradation. *Geophysical Research Letters*, *30*(15), 1808. https://doi.org/10.1029/2003GL017459

Tran, S., Bonsang, B., Gros, V., Peeken, I., Sarda-Esteve, R., Bernhardt, A., & Belviso, S. (2013). A survey of carbon monoxide and non-methane hydrocarbons in the Arctic Ocean during summer 2010. *Biogeosciences*, *10*(3), 1909–1935. https://doi.org/10.5194/bg-10-1909-2013

Van Ginkel, C. G., De Jong, E., Tilanus, J. W. R., & De Bont, J. A. M. (1987). Microbial oxidation of isoprene, a biogenic foliage volatile and of 1, 3-butadiene, an anthropogenic gas. *FEMS Microbiology Ecology*, *45*(5), 275–279. https://doi.org/10.1111/j.1574-6968.1987.tb02377.x

Vlieg, H. J. E. T., Kingma, J., van den Wijngaard, A. J., & Janssen, D. B. (1998). A glutathione S-transferase with activity towards cis-1, 2-dichloroepoxyethane is involved in isoprene utilization by Rhodococcus sp. strain AD45. *Applied and Environmental Microbiology*, 64(8), 2800–2805. https://aem.asm.org/content/64/8/2800/article-info

Wanninkhof, R. (1992). Relationship between wind speed and gas exchange over the ocean. *Journal of Geophysical Research*, *97*(C5), 7373. https://doi.org/10.1029/92JC00188

Wingenter, O. W., Haase, K. B., Strutton, P., Friederich, G., Meinardi, S., Blake, D. R., & Rowland, F. S. (2004). Changing concentrations of CO, CH4, C5H8, CH3Br, CH3I, and dimethyl sulfide during the Southern Ocean iron enrichment experiments. *Proceedings of the National Academy of Sciences*, *101*, 8537–8541. https://doi.org/10.1073/pnas.0402744101

Wurl, O., Wurl, E., Miller, L., Johnson, K., & Vagle, S. (2011). Formation and global distribution of sea-surface microlayers. *Biogeosciences*, *8*(1), 121–135. https://doi.org/10.5194/bg-8-121-2011

Yvon-Lewis, S. A., Butler, J. H., Saltzman, E. S., Matrai, P. A., King, D. B., Tokarczyk, R., et al. (2002). Methyl bromide cycling in a warm-core eddy of the North Atlantic Ocean. *Global biogeochemical cycles*, *16*, 88–1–88–6. https://doi.org/10.1029/2002GB001898

Zeinali, N., Altarawneh, M., Li, D., Al-Nu'airat, J., & Dlugogorski, B. Z. (2016). New mechanistic insights: Why do plants produce isoprene? *ACS Omega*, *1*, 220–225. https://doi.org/10.1021/acsomega.6b00025

Zinser, E. R. (2018). The microbial contribution to reactive oxygen species dynamics in marine ecosystems. *Environmental Microbiology Reports*, *10*(4), 412–427. https://doi.org/10.1111/1758-2229.12626